UC-411
LBL-27420

Lawrence Berkeley Laboratory
UNIVERSITY OF CALIFORNIA

Accelerator & Fusion Research Division

To be published as a chapter in **Biophysics and Synchrotron Radiation**, S. Hasnain, Ed., Ellis Horwood Limited, Chichester, UK

Soft X-Ray Imaging for the Life Sciences

M.R. Howells

June 1989

For Reference

Not to be taken from this room

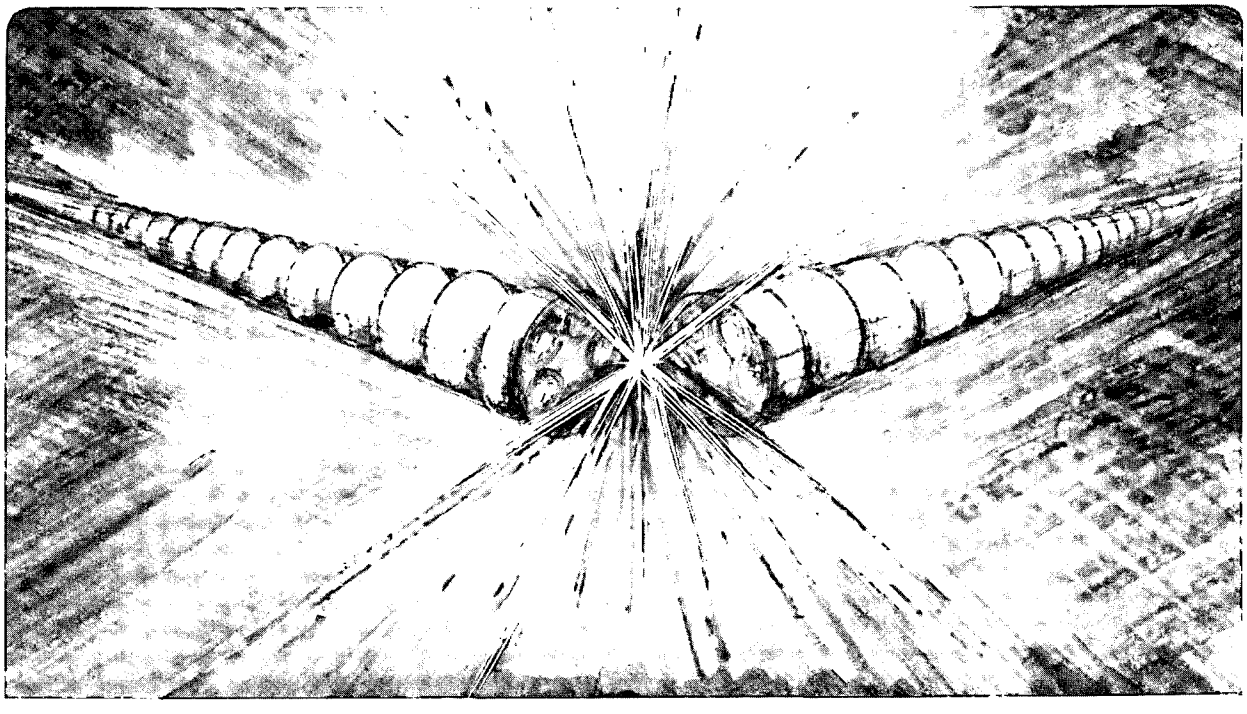

LBL-27420 Copy 1 Bldg. 50 Library.

Prepared for the U.S. Department of Energy under Contract Number DE-AC03-76SF00098.

DISCLAIMER

This document was prepared as an account of work sponsored by the United States Government. While this document is believed to contain correct information, neither the United States Government nor any agency thereof, nor the Regents of the University of California, nor any of their employees, makes any warranty, express or implied, or assumes any legal responsibility for the accuracy, completeness, or usefulness of any information, apparatus, product, or process disclosed, or represents that its use would not infringe privately owned rights. Reference herein to any specific commercial product, process, or service by its trade name, trademark, manufacturer, or otherwise, does not necessarily constitute or imply its endorsement, recommendation, or favoring by the United States Government or any agency thereof, or the Regents of the University of California. The views and opinions of authors expressed herein do not necessarily state or reflect those of the United States Government or any agency thereof or the Regents of the University of California.

LBL-27420

Soft X-Ray Imaging for the Life Sciences*

M. R. Howells

Advanced Light Source
Accelerator and Fusion Research Division
Lawrence Berkeley Laboratory
One Cyclotron Road
Berkeley, CA 94720 USA

* This work was supported by the Director, Office of Energy Research, Office of Basic Energy Sciences, Materials Sciences Division of the U. S. Department of Energy under Contract No. DE-AC03-76SF00098

SOFT X-RAY IMAGING FOR THE LIFE SCIENCES

By M. R. Howells,
Advanced Light Source, Lawrence Berkeley Laboratory, Berkeley, CA 94720, USA

INTRODUCTION

X-ray imaging in its widest sense includes a broad range of endeavors from crystallography to tomography and clinical shadow photography. In this article we deal with the restricted class of imaging experiments in which soft x-rays are used to study biological material at the cellular or subcellular level. In other words, we are concerned with microscopy using x-rays. This subject has a long history but is making particularly rapid progress at the present time.

The successful use of x-rays in so many branches of research bodes well for their utility in microscopy and indeed the x-ray imaging methods that are now emerging offer a rich and complex network of opportunities for life-science researchers. The biology community is only just beginning to study the sample preparation methods and measurement techniques that will be needed to exploit these new possibilities.

One naturally tends to compare the situation to the earliest days of development of the electron microscope. In those days the prospects for life science studies with the new instrument were considered to be very limited by all but a few enthusiasts on account of the expected burning of the sample by the beam. Dennis Gabor, whose studies of the problem of spherical aberration in the electron microscope led him to the discovery of holography and the Nobel prize in physics, characterized the pioneering efforts of L. Marton in biological electron microscopy by the phrase "let it burn but let us look at the cinder" [1]. Nevertheless, efforts to exploit the new instrument for biology continued and we now know that the gloomy prospects of those early years have undergone a remarkable transformation, thanks to the ingenuity of the intervening generations of researchers.

One expects that the same kind of creativity will be needed to take full advantage of the opportunities presented by x-ray imaging techniques, and no doubt there will be similar scepticism until the best application areas have been identified and proved. However, there is reason to hope that the process will move a good deal faster this time. The community has greater resources now in both material terms and accumulated wisdom, and, as we explain later, samples can be imaged or microanalyzed by x-rays with less exercise of ingenuity than is needed for electron or proton probes.

Of course all strategies for exploiting imaging techniques begin with an understanding of the physics of the interaction of the probing radiation with the sample and of the resulting image contrast, and it is this which forms the main theme of this article. We first briefly review the history of x-ray imaging and then discuss the physics of the creation of both two and three-dimensional x-ray images, with special emphasis on resolution and contrast. We then give an overview of the four soft-x-ray imaging techniques that havedemonstrated sub-optical resolution at the present time and provide some explanation of how they work, and their present and projected capabilities. Finally, we give some rather general results on the matter of

the radiation doses involved in obtaining information about the sample.

There is a considerable literature associated with this field. Five conferences have been dedicated to it [2,3,4,5,6], and several recent reviews have been published [7,8,9,94,95]. There are also reviews and conference proceedings from the pre-1970 period that contain sections on x-ray imaging [10]. The book by Cosslett and Nixon [11] provides an excellent treatment of the background against which modern developments have been taking place.

THE WIDER CONTEXT OF X-RAY IMAGING

The three main structural methods used currently in the life sciences are visible light microscopy, electron microscopy and x-ray diffractive techniques including crystallography. All of these have been enormously successful within their domains of application and together have supported the great advances in the understanding of cellular processes which have been characteristic of modern biology. However, the capabilities of the above three methods are not so complete that there is no desire for more. In fact, analysis of the structural studies that have been done reveals that there has always been some need to compromise between fidelity and resolution. Thus the light microscope has the best ability to study natural, even living material but the most severely restricted resolution capabilities. Conversely electron microscopy has outstanding resolution but requires samples to be in non-biological form so that constant attention must be paid to the issue of fidelity in interpreting the features seen in micrographs. One can also make somewhat similar arguments about x-ray diffractive techniques which give the best high resolution information for the class of materials (crystals) that are furthest from natural, biological material.

We believe that the overall capability of this family of structural techniques can be enhanced by the introduction of soft x-ray methods which occupy an intermediate position in the spectrum of the fidelity-resolution trade-off. Thus, x-rays in the spectral range 10-50 Å can make images which have improved resolution compared to the light microscope and improved fidelity compared to the electron microscope. Indeed, such x-rays can image samples which, apart from the fact of illumination by an x-ray beam, are in their natural state, in an aqueous environment and in atmospheric pressure air, just as they would be on the stage of a visible light microscope. The resolution of such images enables much of the structure in the size range .05-1.0 micron to be imaged at the present time with prospects of improvements toward .01 micron in the reasonably near future. The fact that there is great interest in these kinds of studies can be inferred from the scale of the response to the recent progress that has been made in confocal visible light microscopy.

The physics of the interaction of soft x-rays with matter is different from that of the other probes and this leads to some advantageous imaging properties. The spectral region between the Ok edge (24 Å) and the Ck edge (44 Å) has the special property that carbon and nitrogen containing materials give absorption contrast whereas water is relatively transparent. This region is therefore known as the "water window" and is the origin of the claimed ability to study objects in an aqueous environment. Soft x-rays also have about the right penetrating power to interact with an intact cell and provide a measurable transmitted or diffracted signal. Because of the resonant

interaction with atoms near x-ray "edges", monochromatic x-rays in general can be used to create core holes with improved selectivity and therefore contrast in absorption or fluorescence microanalysis. As we shall see later, improved contrast leads directly to a lower dose for a given task.

Fig 1 shows a comparison of some of the contrast properties and the penetration of soft x-rays and electrons in the respective energy regions in which they are often used for imaging. One can see that the x-rays show more contrast between biological material and water and higher penetration than electrons. These characteristics can be translated into an ability to utilize the natural contrast of the native material and to avoid dehydration, sectioning, staining, embedding, freezing and all forms of radical modification of the sample. All the methods of x-ray imaging discussed here can, in principle, be implemented with the sample in a "wet cell" in liquid water at atmospheric pressure and most of them have been [12]. However. one should not think that this is a trivial thing to arrange. Providing suitable thin windows, controlling the thickness of the water layer and, in cases where synchrotron radiation is involved, dealing with a vertical sample-plane, requires considerable effort and care.

HISTORY [13]

The first successful attempts to form x-ray images were made almost immediately after the discovery of x-rays in 1895. A photographic plate was exposed to x-rays through a sample that was in contact with it [14]. The plate was then developed and the resulting pattern, known as a "contact microradiograph" was examined in the light microscope.

To achieve resolution superior to that of the light microscope was apparently possible in principle but without a source of submicron dimensions, a submicron resolution detector or an optical system that could provide enough magnification, further improvements to the x-ray microscope were blocked for several decades. The first successful x-ray lens was reported by Kirkpatrick and Baez in 1948 [15] and marked the beginning of a long struggle which still continues today to solve the technical problems involved in producing a high-resolution x-ray microscope objective. The Kirkpatrick-Baez scheme involved two spherical mirrors working at extreme grazing incidence and arranged so that the plane of incidence of the second was perpendicular to that of the first. In this way, each mirror provided focussing in one plane and, to first order, did nothing in the other. The method was successful in making magnified x-ray images but was prevented by aberrations and surface finish considerations from achieving resolution superior to that of the light microscope. Subsequently more advanced manufacturing methods have been tried but so far without achieving submicron resolution. All methods based on reflection have now been eclipsed in resolution by the Fresnel zone plates that are currently being made and we return to this subject later.

A different approach, developed in the 1950's was the so called "projection microscope" [16]. In this instrument an electron microscope-type focussing system was used to produce a small focal spot on the anode of an x-ray tube. This "microfocus" x-ray source was placed in front of the sample and a photographic plate was placed a considerable distance behind it. The plate recorded a magnified projection of the sample limited in resolution mainly by diffraction. This system reached the point of commercial production [11] and even now continues to produce many interesting pictures [17].

However, it also has failed to improve on the resolution of the light microscope.

A number of technical developments have occurred in the last decade or two which have led to rapid improvements in the performance of x-ray imaging systems. Among these are the construction of high brightness synchrotron radiation sources, particularly undulators, and the development of sophisticated microfabrication methods (mainly for microcircuits) which have enabled high resolution Fresnel-zone-plate lenses to be made. The latter have been produced by both electron beam writing and by ultraviolet holography. Finally, organic polymers such as polymethylmethacrylate (PMMA) have come into use as high resolution x-ray recording materials (resists). The technology which has not yet had much impact in soft x-ray imaging, but which promises a good deal in the not-too-distant future, is the imaging solid state detector [48]. Significantly higher resolution detectors than the 25 micron devices available commercially now are said to be technically within reach. If such devices were to become available, they could make a considerable impact on x-ray imaging techniques.

RESOLUTION: TRANSVERSE AND LONGITUDINAL

The resolution of any optical system can be discussed in terms of its numerical aperture. For reasons of simplicity we give this discussion for a rectangular aperture and make use of the small angle approximation. The point spread function for such an aperture, normalised to unity at x=y=0, is given by

$$P(X,Y) = \sin(X)/X \, \sin(Y)/Y$$

where $X=k_o ax/f$, $Y=k_o ay/f$ with $k_o=2\pi/\lambda$, a equal to the half-width of the aperture and f the focal distance. Since the x and y parts are separable we consider the x part only from now on. We define the transverse resolution d_x to be equal to the distance from the center to the first zero of sin(X)/X. which is the x value for which $X=\pi$

$$d_x = 0.5 \; \lambda/NA \qquad (1)$$

where the numerical aperture (NA) of the system is defined as the sine of the half-angle subtended by the aperture. (NA=a/f in our approximation.) Similarly for d_y. One can see that this procedure is very similar to the definition of the Rayleigh resolution for a circular aperture which is 0.61 λ/NA.

The maximum spatial frequency, W, accepted in the x direction, by our system is NA/λ and so the resolution is given by (1) as half of one period of that frequency. This defines a relationship between resolution and frequency that we will use later.

We now consider the way in which an optical system with numerical aperture NA obtains information in the depth (z) direction. The elastic scattering of a wave must obey Bragg's law

$$\mathbf{K} = \mathbf{k}_o - \mathbf{k} \qquad (2)$$

where $\mathbf{k}_o$ and $\mathbf{k}$ are vectors of magnitude k_o and the directions of the inward and outward photon respectively. K is a vector representing a periodicity

(Fourier component), of wavelength $2\pi/|\mathbf{K}|$, in the sample which is responsible for the scattering and is being detected by it. For a given ingoing vector $\mathbf{k}_o$, the various outgoing beams, $\mathbf{k}$, are probing a range of values of $\mathbf{K}$, given by (2). From the geometry of the vector diagram one can see that the probed $\mathbf{K}$ values lie on a sphere (the "Ewald" sphere)[18] of which the $\mathbf{k}_o$ vector is a radius (Fig 3). The equation of the sphere is

$$K_x^2 + K_y^2 + (K_z + k_o)^2 = k_o^2$$

For an extreme ray (K_x=NA/λ, K_y=0) in the small angle approximation this gives

$$K_z = -NA^2/2k_o \tag{4}$$

If we use the same definition of the relationship between resolution and frequency that we had before this leads to a value for the depth resolution dz

$$d_z = \lambda/NA^2 \tag{5}$$

When two of the smallest resolvable elements are positioned to be just resolved according to the above criterion, their separation is d_x.
This leads to a rough picture of the smallest resolvable element as an ellipsoid of revolution with semiaxes $d_x/2$, $d_y/2$ and $d_z/2$ and volume V_c given approximately by

$$V_c = 2d_x^4/\lambda \tag{6}$$

That the element is stretched out in the depth (z) direction is a reflection of the much poorer resolution in that direction, of microscopes (including all x-ray microscopes) that have NA values much less than unity.

It is also possible to consider this ellipsoid in another way. It is the volume from within which rays reach a receiving point at (x=a, y=0) at the edge of the aperture with no more than a phase change of $\pi/2$ relative to a ray from the center point. This is based on two-dimensional geometrical arguments. Displacements of a point scatterer by d_x transversely or d_z longitudinally, each give $\pi/2$ phase change at the receiving point. There is, therefore, a sense in which the resolvable volume element is also the element which scatters coherently to all points within the aperture that was used in defining it. One can understand this at the level of a two-dimensional element in the x,y plane by comparing the forward process; ideal imaging through the aperture to give the point spread function (ie the resolution element), and the reverse process; scattering back into the aperture by an object with scattering strength distribution given by the same point spread function. The first is represented by a Fourier transform (Fraunhofer diffraction) while the coherence aspect of the second is represented by the corresponding reverse transform (Van Cittert-Zernike Theorem [19]). The original aperture thus reappears as the modulus of the complex coherence factor [19] of the resolution element or in other words as its "coherence patch". It seems plausible that this two-dimensional argument could be extended to cover the three-dimensional case we are dealing with here.

PHYSICS OF X-RAY IMAGING

All methods of x-ray imaging involve illumination of the sample with x-rays and utilization of the emerging wavefield to obtain information about the sample structure. Therefore we need a suitable physical description of the interaction of x-rays with the kinds of samples we are interested in. Suppose we represent the electric field vector of the x-ray beam by $\mathbf{E}(\mathbf{r})$. We know that E (representing any of E_x, E_y or E_z) must satisfy the Helmholtz equation

$$\nabla^2 E + k^2 E = 0 \tag{7}$$

where a sinusoidal time dependance has been assumed. We can rewrite this by noting that $k = nk_o$ where $n = 1 - \delta - i\beta$ and is a function of position. Thus $\mathbf{n}(\mathbf{r})$ is the unknown, complex sample function that we are trying to find.

$$\nabla^2 E + k^2 E = (1 - \mathbf{n}^2) k_o^2 E = UE \tag{8}$$

The solution of this equation [20] in three dimensions can be written as an integral equation as follows (see fig. 2):

$$E(\mathbf{r}) = e^{ik_o d} - \frac{1}{4\pi} \int_{\text{sample}} \frac{\exp ik_0 |\mathbf{r} - \mathbf{r}'|}{|\mathbf{r} - \mathbf{r}'|} U(\mathbf{r}') E(\mathbf{r}')\, d^3\mathbf{r}' \tag{9}$$

In words, each element $d^3\mathbf{r}'$ of the sample depletes the incoming wave by scattering a secondary wavelet of strength $(-1/4\pi)E(\mathbf{r}')$ times the amplitude incident on the element. If the sample is both a weak scatterer and a weak absorber, then one can consider that each element is illuminated by the unmodified incident beam, so that $E(\mathbf{r}')$ can be replaced by a constant. This is the Born approximation. In this case equation (9) is evidently a convolution integral of the sample "potential" $U(\mathbf{r}')$ with the shift-invariant impulse response (Greens) function of the problem, $\exp ik_o r/r$. This is the starting point for the analysis of three-dimensional imaging using multiple illumination directions (diffraction tomography) which is considered later. If we imagine that the sample in fig. 2 shrinks down to a flat two-dimensional sheet perpendicular to the incoming beam then with $|\mathbf{n}-1| \ll 1$, $U(\mathbf{r}')dz$ reduces to something like a complex transparency. If, in addition, we assume the sample occupies an aperture in an otherwise infinite, opaque screen and, following Kirchhoff, make assumptions about the boundary conditions to be applied at the aperture-plus-screen, then the problem can be analyzed by the standard analysis of Fourier optics. The signal at Q is then given in the Fresnel approximation by [21]

$$E_Q(\mathbf{r}) = \frac{e^{ik_o d}}{i\lambda d} \int_{\text{sample}} T(x', y') \exp \frac{ik_0}{2d} \left[(x - x')^2 + (y - y')^2\right] dx' dy' \tag{10}$$

The validity criteria for the Fresnel approximation are generally well satisfied in x-ray optics on account of the relatively low (<1/10) numerical aperture of most of the systems so far built.

The sample is represented in all these treatments as a complex refractive index distribution. This represents the optical properties of the material in a way that is most simply stated for a pure element whose atoms scatter like $f = f_1 + if_2$ electrons where f_1 and f_2 are tabulated for all elements for essentially all the x-ray and soft x-ray region [22]. The refractive index n is given by

$$n = 1 - \delta - i\beta$$
$$\delta = Qf_1,\ \beta = Qf_2,\ Q = r_o n_o \lambda^2/2\pi \tag{11}$$

where r_o is the classical eletron radius, n_o is the number of atoms per unit volume and δ, $\beta \ll 1$ in the spectral region of interest to us.

Consider now a homogeneous material composed of n_m molecules per unit volume, each with q_j atoms of type j and integrated scattering factor $F_m = F_{1m} + iF_{2m}$. (We take as a convention that capital F's refer to the scattering factors of objects larger than atoms such as molecules, sample resolution elements etc. It is further assumed that the objects are still small enough to scatter coherently so that the F's are simply found by scalar addition of the f's of the constituent atoms.) In this case for material comprising the substance m alone

$$n_M = 1 - \frac{n_M r_0 \lambda^2}{2\pi} \sum_j q_j (f_{1j} + i f_{2j}) = 1 - \frac{n_M r_0 \lambda^2}{2\pi} (F_{1m} + i F_{2m}) \tag{12}$$

The general behavior of the scattering factors is descriptive of the interaction of x-rays with matter and shows sharp resonances at energies corresponding to atomic shells. Typically the absorption (f_2) resonances look like sharp steps on a log-log plot giving rise to the name "edges" while the f_1 values are high on both sides, with a deep minimum at the edge. This behavior is rooted in the fact that n^2-1 (and for small δ and β, $f_1 + if_2$ as well) can be regarded as the frequency transfer function of a causal system. The electric field is the input and the dipole moment per unit volume or polarization, the output of this system. Therefore, f_1 and f_2 must form a Hilbert transform pair [23]. This fact is used in preparing the tables of f_1 and explains the close analogy that exists between optical behavior and that of other resonant systems. For example, f_1 corresponds to reactive and f_2 to resistive behavior. The limiting behavior of f_1 and f_2 at high photon energies is also of interest and can be derived by realising that for energies far enough above their K resonances, light atoms behave like Z free electrons. f_1 therefore tends toward Z while the f_2 energy dependance is that of the dominant absorption process: photoelectric absorption by the electron gas. This can be shown [24] to give a falloff in the crossection proportional to $(\text{energy})^{-7/2}$, and therefore in f_2 proportional to $(\text{energy})^{-5/2}$. This explains the well-known increase of transparency of light elements at high x-ray energies. At such energies there is, therefore, a dose advantage to using imaging methods with contrast based on f_1.

The two most important physical processes for imaging with soft x-ray photons are thus photoeletric absorption represented by f_2 and coherent (Thomson) scattering represented by f_1. Incoherent (Compton) scattering becomes significant compared to the coherent process, only for energies above about 5 keV. The atomic crossections for all of these processes are extensively tabulated [25]. For both atoms and larger objects scattering coherently, the crossections are related to the scattering factors as follows:

$$\sigma_a = 2 r_0 \lambda F_2 \tag{13}$$

$$\sigma_s = (F_1^2 + F_2^2) r_0^2 \int_0^A \frac{1 + \cos^2 A}{2}\, d\Omega \tag{14}$$

where Ω is the solid angle.

Specializing to the case of a single atom for the moment, we can say that in the soft x-ray region, the electrons in the atom scatter coherently even when the above integral is taken over all angles. σ_s then becomes equal to

the Thomson crossection $8\pi r_o^2/3$ times $(f_1^2+f_2^2)$. When this value is compared to the photoelectric absorption crossection (σ_a), one finds that for light elements σ_a is much larger. For example at 0.5keV [25]

	Carbon	Nitrogen	Oxygen
σ_a(Barns)	2.68E5	4.41E5	3.81E4
σ_s(Barns)	2.33E1	3.19E1	4.19E1

One meaning of this is that one cannot image single atoms by scattering soft x-rays (a fact that is also apparent from diffraction arguments) because the radiation damage is proportional to the absorption while the imaging signal is proportional to the scattering. However, even though the crossection ratio σ_s/σ_a is small for light atoms, we will show below that it becomes much larger for larger objects so that scattering can still be a viable process for imaging. One way to see this is to recognize that microscopy samples are typically about one or a few microns thick, and we can see from fig 1 that this can be about an absorption length for some soft x-ray energies. Now the wave transmitted by a sample of thickness t, can be written

$$e^{-ik_o nt} = e^{-ik_o t} e^{+ik_o \delta t} e^{-k_o \beta t} \tag{15}$$

so the phase change is $\delta k_o t$ and the amplitude change (absorption) is $e^{-(\beta k_o t)}$. From this and the above equations for δ and β, one can see that the phase change per absorption length is $(F_1/2F_2)$ which is quite significant in size: greater than one radian for most of the region above about 0.5 keV for biological material (see table II). This indicates that if the sample has sufficient structural variation, significant transverse phase gradients $d\phi/dx$ can exist in the exiting wave. This indicates scattering by an angle A according to the relation

$$\sin(A) = (d\phi/dx)/k_o \tag{16}$$

Of course samples with no structure still scatter but the scattered waves merely reconstruct the incident wave with a phase change.

Now consider [26] a pixel of scattering factor $F = F_1 + iF_2$ electrons. The scattering crossection is given by equation (14) for small angles

$$\sigma_s = \pi |F|^2 r_o^2 A^2 \tag{17}$$

$$= \pi r_o^2 d^6 s^2 \tag{18}$$

where we have used the expression $2d^4/\lambda$ (6) for the pixel volume. The absorption crossection is given similarly by (13)

$$\sigma_a = 4 r_o d^4 a \tag{19}$$

(s and a are defined in the next section). Thus

$$\sigma_a/\sigma_s = 4a/(\pi r_o s^2 d^2) \tag{20}$$

This shows that the crossection ratio indeed depends on the pixel size and that the number of absorbed photons per scattered one decreases (improves) as the resolution element gets larger, reaching a value of unity, for example, when λ=30 Å, d=200 Å and the material is protein [96]. This opens the door to x-ray imaging experiments based on scattering, in spite of the unfavorable ratio of the atomic crossections.

THEORY OF CONTRAST

The x-ray imaging techniques that we will discuss can utilize at least three forms of contrast: amplitude, phase and coherent scattering. Amplitude and phase contrast are taken to mean the same as for the light microscope with Zernike phase contrast [27] capability while scattering contrast is defined on the understanding that an image of the object will be reconstructed with contrast determined by the local scattering strength. Actually phase delays and scattering are, in part, the same physical effect but are different in our treatment because our scattering includes "shadow scattering"; the scattering resulting from absorption, and because we consider objects of a size and shape to scatter coherently (proportional to the number of electrons squared). Zernike phase contrast, on the other hand, when treated in the usual weak phase approximation, is linearly proportional to the number of electrons in the feature. In terms of generic Henke scattering factors, amplitude, phase and coherent scattering contrast are related to F_1, F_2 and $(F_1^2 + F_2^2)$ respectively. The scattering is dependant on both the f_1 and f_2 contributions from each atom, although in much of the range of interest to us the effect of f1 dominates due to its greater size.

We would like to be able to discuss x-ray imaging in terms of an intrinsic contrast between materials which is related to their microstructure in a quantitative way and does not depend on the thickness and other detailed properties of individual samples. To fix our ideas we will consider the contrast between protein [96] and water, but the method is of wider application. We define an absorption strength a, a phase-change strength ϕ and a scattering strength s which will be expressed in equivalent electrons per cubic Å. Thus

$$a_w = n_w F_{2w}, \qquad a_p = n_p F_{2p} \tag{21}$$

$$\phi_w = n_w F_{1w}, \qquad \phi_p = n_p F_{1p} \tag{22}$$

$$s_w = n_w(F_{1w}^2 + F_{2w}^2), \quad s_p = n_p(F_{1p}^2 + F_{2p}^2) \tag{23}$$

$$s_{pw} = (n_p F_{1p} - n_w F_{1w})^2 + (n_p F_{2p} - n_w F_{2w})^2 \tag{23a}$$

where the F's are the integrated scattering factors for the water and protein molecules defined earlier and the n's are the number of molecules per unit volume. s_w and s_p correspond to isolated fragments of each material while s_{pw} is the excess scattering strength of a protein fragment relative to water in which it is intimately embedded. In the latter case the protein-water difference signal must be calculated by subtracting amplitudes. The "intrinsic contrast", C, is now defined as the difference of the strengths of the two materials divided by the strength of the "background" which is

considered to be water in the present case. Thus

$$C_a = (a_w - a_p)/a_w \tag{24}$$

$$C_\phi = (\phi_w - \phi_p)/\phi_w \tag{25}$$

$$C_s = s_{pw}/s_w \tag{26}$$

These measures of intrinsic contrast can be calculated easily from the Henke scattering factors and allow one to study issues such as the choice of wavelength and contrast mechanism for given experiments in a rational way. They are also in the right form for use in applying the Rose criterion in dose calculations (see later).

An example of a contrast mechanism is shown in fig 4 where the scattering strength of protein, water and protein against a background of water are plotted. One can see that although the incoherent difference in scattering strength can be either positive, negative or zero, the coherent difference (eq. 23a) is never negative and can only become zero if the F_1 and the F_2 terms BOTH vanish at the same wavelength.

A more complete picture of the options for choice of wavelengths and contrast mechanisms is provided in fig 5. There the contrast due to the three mechanisms is shown as a function of wavelength for imaging protein against a background of water. One can see clearly the advantages of using the water window wavelengths with amplitude (absorption) contrast. However such contrast below 24 Å is close to zero and much less promising. The value of phase contrast becomes evident, particularly for wavelengths shorter than 24 Å, while there is an indication that a wavelength just above that of the oxygen edge may be a good choice for scattering experiments.

PHASE CONTRAST

It can be seen from fig 5 that there are considerable possibilities for using phase contrast in x-ray imaging. However, although there had been considerable study given to the use of phase effects in zone plate design [28], their use in imaging experiments does not seem to have been discussed until the recent work of Schmahl and Rudolf [29] first reported in 1986. These authors point out that phase contrast can be implemented with an imaging x-ray microscope using methods that we will shortly describe and that it has important advantages. The chief one is that one can consider doing x-ray imaging at shorter wavelengths than hitherto so that perhaps the region 5-25 Å becomes open for microscopy and without the use of resonant effects. At such wavelengths, f_1 remains high while f_2 diminishes rapidly leading to a general improvement in the information to dose ratio which we will consider in more detail later. Other conveniences are a reduction in the absorption losses at windows, gas layers, support films etc and an ability to examine thicker specimens.

Objects which absorb no light are generally invisible in the light microscope even if they induce phase shifts in the transmitted radiation. This is because the microscope provides only the intensity and not the phases of the image. This problem was addressed in the original work of Zernike [27] by providing a $\pi/2$-phase-shifting plate in the back focal plane of the objective lens as shown in fig 6. The method depends for its success on

coherent illumination. The phase plate can be considered as a filter of transmission T(u) given by

$$T(u) = i \quad |u|<\epsilon \qquad (27)$$
$$\quad = 1 \quad |u|>\epsilon$$

where $\epsilon \ll 1$. We are taking the spatial coordinate x and the corresponding frequency u to be representative of two dimensional systems. Suppose the object is given by

$$f(x) = \exp(i\phi(x)) \simeq 1 + i\phi(x) \qquad (28)$$

The weak phase approximation is used here for simplicity although it is not valid over the whole spectral range of interest. The amplitude distribution in the back focal plane is the transform F of f.

$$F(u) = \delta(u) + i\ \Phi(u) \qquad (29)$$

After passage through the filter this becomes

$$G(u) = F(u)T(u) = i\ \delta(u) + i\ \Phi(u) \qquad (30)$$

Now taking the transform to get the final image we have

$$g(x) = i\{1 + \phi(x)\} \qquad (31)$$
$$|g(x)|^2 = 1 + 2\phi(x)$$

Even better we could have $T(u) = \alpha i$ instead of i where α is some absorption factor. The final result would then be

$$|g(x)|^2 = \alpha + 2\phi(x) \qquad (32)$$

an improved contrast solution. Still further refinements can be made by generalizing the "disk" represented by (27) to a ring [30]. The essence of Zernike's concept is that one starts with two vectors, 1, and a much smaller one, $\phi(x)$, that are perpendicular in the Argand plane (28). The magnitude of the resultant is therefore indistinguishable from unity. The effect of the filter is to rotate the vector, 1, to be parallel (or antiparallel) to the $\phi(x)$, so that the magnitude of the resultant now has a first order difference from unity.

There are a number of practical difficulties in implementing phase contrast. One is the need for the phase plate to be of finite size. This is an issue in visible light systems as well and has been widely studied The effect is to create a halo artifact around point-like objects [30] or a fringe on each side of a step-like one [31]. Another problem is to produce the right amount of phase change. A way to simplify the making of the phase plate would be to make it fully opaque (central dark field method). The result of the above calculation would then be $g(x) = i\ \phi(x)$, $|g(x)|^2 = \phi(x)^2$. One price of the simplification is that g(x) is no longer a linear mapping of $\phi(x)$. However, considering how difficult x-ray imaging experiments are and how easy digital image processing is becoming, this is apparently not as compelling an argument as it once was. Another method with the same tradeoff

of linearity against simplicity is the Schlieren method. For this one simply blocks half of the aperture (say the x<0 half). The result in this case is [21]

$$|g(x,y)|^2 = 1/4\{1 - 2\phi_{hx}(x,y)\} \tag{33}$$

where $\phi_{hx}(x,y)$ is the Hilbert transform of $\phi(x,y)$ with respect to x.

We have not exhausted the methods for generating phase contrast. In fact ANY modification of the system aperture will produce some degree of phase contrast. An example of such modification is an aberration (ie a distortion of the complex aperture function) and an important case widely used in electron microscope imaging is defocus. This is less attractive in x-ray microscopes because of the loss of resolution that would be involved. Nor is the imaging x-ray microscope the only kind that can be used to give phase contrast. Any experiment that uses the diffracted wavefield, automatically uses contrast that includes both amplitude and phase effects (eg holography) while the scanning x-ray microscope, like its optical counterpart is potentially able to record phase contrast if it is operated with a split detector [32].

In 1988 the Gottingen group reported successful imaging experiments using Zernike phase contrast [33,34]. These employed silver or gold phase plates and involved several different biological samples. The performance in terms of resolution and imaging speed appears to be similar to amplitude contrast pictures made at the same wavelength (45 Å). Plans for further experiments with improved coherence and shorter wavelengths exist and should provide an even better demonstration of the advantages of the concept.

FLUORESCENCE CONTRAST

It is not part of our main theme to consider microanalysis but we include a brief comment on it for completeness. The subject has been treated rather thoroughly in a series of papers by Kirz [35,36,37]. Fluorescence contrast is useful and well matched to x-ray excitation for elements above about 20. The fluorescent yield increases with Z approximately as $Z^{3.3}$, passing the value 0.1 at Z=17. For low Z elements core holes relax predominantly via the competing Auger process. The best technique for fluorescence microanalysis is to excite the sample by means of a focussed monochromatic x-ray beam, tuned to the appropriate atomic resonance. Such an illumination can now be done with high flux and a spatial resolution of a few microns. There are also prospects for using zone plates to get resolution considerably below one micron [38]. The resonant character of x-ray absorption plus the absence of Bremsstrahlung and virtual absence of inelastic scattering of the primary beam guarantee a high selectivity in excitation and low background. This leads to detectability thresholds that are very low and generally superior, on a dose-for-dose basis, to those obtained with electron, proton or white x-ray beams [36,39].

For atoms with atomic number below about 20 the rapid falloff of the yield deprives the fluorescent method of its dose advantage, and electron energy loss spectroscopy and differential x-ray absorption become the methods of choice for microanalysis [36].

As an example of the quantitative results of Kirz [37] one can say that, under reasonable assumptions about the capability of the detectors, the dose needed to detect a mass (M)=1 femtogram of material by K fluorescence

excited by monochromatic x-rays varies from about 10 Mrad at Z=40 (zirconium) to 100 Mrad at Z=16 (sulfur). Within certain limits, the dose required is proportional to 1/M and independent of the size of the area within which the detected mass is distributed. Translating this into concentration terms, it should be possible to detect millimolar sulfur resolved to $1\mu m^3$ by means of a dose of $3x10^9$ rads. Scaling to either micromolar sulfur or $0.1\mu m^3$ would require 1000 times less mass and therefore 1000 times more dose.

X-RAY SOURCES

The requirements for x-ray sources for microscopy have received a good deal of study. The main point is that for many experiments, the x-ray beam must be spatially and temporally coherent. This requirement could not be satisfied by x-ray tube sources but in modern times has been satisfied to a useful extent by synchrotron radiation sources. At the present time the most useful type of source for microscopy is an undulator on a low emittance storage ring. Short wavelength lasers also provide excellent sources at certain wavelengths and are beginning to be used for imaging. They have excellent temporal coherence and can, in favorable cases, make an image with a single, subnanosecond pulse. If this is the intention, a laser source for imaging needs to provide enough photons with sufficient spatial and temporal coherence per pulse to make an image. This goal has been reached by the present generation of x-ray lasers for wavelengths 206, 209 [40] and 182 [41] Å. It has not yet been reached for water window and shorter wavelengths, although rapid progress toward it is being made.

The coherence properties of electromagnetic fields have been treated by a number of texts [19] and articles [42] and usually the spatial and temporal aspects are considered separately.

The temporal coherence is described by a coherence length (l_c) which is roughly the length of the electromagnetic wavetrain. It is formally defined as the amount of path difference which could be tolerated between the beam and a replica of itself for a given loss of fringe contrast when the two are imagined to be interfered. Such a thought experiment could in principle be realized by an amplitude division interferometer. l_c is closely related to the monochromaticity $\lambda/\Delta\lambda=N$ and one has $l_c=N\lambda=\lambda^2/\Delta\lambda$. In synchrotron radiation practice, temporal coherence requirements normally demand a monochromator, even for undulator sources which are quasimonochromatic. In zone plate experiments the needed resolution is given by $\Delta\lambda/\lambda$ roughly equal to the number of rings of the zone plate. In holography there is actually a path difference between two interfering beams to which l_c must be matched.

The spatial coherence is defined similarly except that it is two transversely separated points on the wavefront from which signals are imagined to be taken for an interference experiment. The region of spatial coherence (the coherence "patch") is that over which the pairs of signals would give fringes of some given contrast. The process could be realized this time by a wavefront division interferometer. Exact details of the phase space of spatially coherent beams are provided, for example, in [43], but if we ignore proportionality constants of order one we can say that the coherence patch subtends an angle of roughly λ/s at the source where s is the source size. If the source emits only into the coherence patch it is said to be fully spatially coherent or single-mode. From this it is apparent that a single-mode beam such as that from a well-prepared visible-light laser has an emittance

(width times angular width) of about λ. The phase space volume of a coherent beam, including both transverse directions, is thus about λ^2. For sources that are not single-mode such as all the x-ray sources, both laser and synchrotron radiation, operating at present, the only way to obtain the single-mode source needed for most imaging experiments is to use apertures to block all the light from the source except that in the coherence patch.

Since the degree of spatial coherence drops off gradually with increase of the distance between the two sample points, it is necessary to adopt an criterion for how much beam to accept in an experiment. The most important case is illumination of a zone plate, where lack of spatial coherence in illuminating the various zones will cause a loss of resolution. On the other hand, too much spatial coherence (utilization of only part of the mode) causes a loss of flux. Calculations show that if the source is approximated by an incoherently illuminated circular pinhole, then a good resolution flux trade-off is obtained by accepting a cone of full angle equal to half the width of the ring (the "Airy disc") due to the first zero of the diffraction pattern of the pinhole.

For a synchrotron radiation source the figure of merit for imaging is generally the spectral brightness (B) [43] which is usually expressed in photons/sec/mm^2/mr^2/0.1% bandwidth. B is thus the flux per unit bandwidth per unit phase space volume (see fig 7). The part of the flux that is spatially coherent is the part in a phase space volume λ^2 so the spatially coherent flux per unit bandwidth is $B\lambda^2$. If a given coherence length is required, then the bandwidth becomes λ/l_c leading to a coherent flux of $B\lambda^3/l_c$, demonstrating the extremely high values of B that are needed for coherence experiments in the harder x-ray regions.

Synchrotron radiation and laser sources are not the only sources that can be used for x-ray imaging. If the coherence requirements are low, then x-ray tubes, laser-heated plasmas and gas discharge sources can be quite effective.

OVERVIEW OF X-RAY MICROSCOPE TECHNIQUES

In this review we will limit our consideration to those x-ray microscopes which have demonstrated resolution superior to the visible light microscope. This limits our consideration to four soft x-ray schemes; contact x-ray microscopy [44], imaging x-ray microscopy [45], scanning x-ray microscopy [46] and x-ray holography [47]. These methods are all patterned after well-known optical techniques: contact printing, conventional optical microscopy, scanning optical microscopy and visible light holography. Where lenses are required, Fresnel Zone Plates [28,68] are used and the technology of these devices is one of the factors that favors the use of fairly soft x-rays in high resolution x-ray imaging. The resolution of a zone plate lens is roughly equal to the spacing of the finest (outer) zones, which must therefore be made small. This sets a practical limit to the thickness, so that zone plates work best below about 1 keV and only poorly at greater than about 5 keV [38]. There are other ways to focus hard x-rays and there are some higher energy techniques; especially microtomography [48] and the scanning x-ray microprobe [49] that we hope will soon enter the suboptical regime.

The PUBLISHED capabilities and special characteristics of the four methods listed above are summarised in Table 1 which is intended to give some idea of the stage of historical developement of these technologies. In many cases performance values beyond the published ones in the table have already

been achieved but we make the "published" stipulation to give uniformity for comparison purposes. All of the methods can be configured to provide imaging of wet, unfixed, unstained, unsectioned, biological objects up to several microns in thickness. The achieved resolution at present is in the range 200-630 Å for all of the methods.

At the present time progress in three dimensional imaging by any of the methods has only just begun [8], although the issue is the subject of considerable study. The imaging and scanning microscopes can try to make

TABLE I
CHARACTERISTICS OF SOFT X-RAY IMAGING TECHNIQUES

CHARACTERISTIC	CONTACT	IMAGING	SCANNING	HOLOGRAPHY
Achieved res'n with good contrast sample (Å)	200	500	500	630
Dose at above res'n imaging C & N (Mrads)	50	10-60	1	200
Exposure: bend magnet	5 min	10-100 sec	1 hour	1 day
undulator	few sec		2 min	1 hour
Coherent source needed ?	no	no	yes	yes
$\lambda/\Delta\lambda$ needed	3	300	300	500
Type of contrast normally	amplitude	amplitude	amplitude	amplitude and phase
Arrangement to get phase contrast	not possible	done by frequency plane filters [29,33,34]	potentially doable by split detector[32]	happens naturally
Potential for quantitative microanalysis	poor	potentially doable by differential absorption	done by differential absorption,[51] potentially doable by fluorescence	poor

"optical sections" [50] just like their optical counterparts and holography is known to have a potential for three dimensional images. The difficulty in all cases is the poor numerical aperture (NA) of the experiments. This matter is considered further in a later section.

The poor numerical aperture (spatial frequency bandwidth) of the experiments translates to a resolution that is many times the x-ray wavelength. The apparent similarity of all the methods in this respect can be traced to a common root: the dependance on the properties of x-ray resists, especially polymethylmethacrylate (PMMA) [52,53]. Resist is used in all presently-favored methods of zone plate manufacture and is directly involved in contact microscopy and holography. The ultimate, useful resolution of PMMA is probably about 100 Å and this sets a limit to the resolution one can expect to achieve by further refinement of these methods. Strategies for changing the methods to circumvent the limit are, of course, under study and are described in the next three sections.

CONTACT MICROSCOPY

This is so far the most popular form of x-ray microscopy [12,44,54] and the one which has been most widely tried on biological applications. It is the modern counterpart of the early method called x-ray microradiography which used photographic film as a detector. The present-day method is based on the idea of Ladd, Hess and Ladd [55] in its use of radiation damage as a way to make a high resolution record of an x-ray wavefield. However, the application of this concept to practical microscopy was pioneered by R. Feder, D. Sayre, E. Spiller and colleagues at the IBM, Thomas J. Watson Reseach Center [56,57]. The method achieves high resolution by use of x-ray resists such as polymethylmethacrylate (PMMA) which were introduced originally for electron beam lithography. The resist is exposed to the x-ray beam through the sample and thus gives a shadow picture limited in resolution by the intrinsic resolution of the resist (largely determined by electron range) and by diffraction. Since electron range increases at higher photon energies while diffraction increases for lower ones, there exists an optimum energy which is conveniently around 250 eV for PMMA [53]. This makes water window experiments near optimal in this respect. The diffraction limited resolution is roughly given by $(\lambda z)^{1/2}$ where z is the feature-to-resist distance. This is a significant effect for all sample distances greater than about 400 Å which means most practical cases.

After exposure the resist is developed, usually in methylisobutyl ketone diluted with isopropanol which transforms the x-ray damage distribution into a relief pattern in the resist with reasonable fidelity. For positive resists, like PMMA, the highest exposure areas are the most soluble. In order to preserve high resolution the pattern is read either by a scanning electron microscope or, better, by a transmission or scanning transmission electron microscope. In the latter cases the resist must be mounted on a thin membrane such as a silicon nitride window [58] and may also be glancing-incidence shadowed with heavy metal. The readout step [59] is not an easy one because resist, even with metallization, is not stable under the electron beam. An alternative approach to the readout problem is to use a replica, either of metal [44] or plastic [60], with superior electron microscopy properties to PMMA. An even better method, which has been demonstrated for readout of holograms, but would work equally well here, is the use of an atomic force microscope to obtain a quantitative readout directly into a computer memory [61].

Contact microscopy is very undemanding on the spectral and spatial properties of the illuminating beam and thus it can be implemented with a

simple x-ray tube or a single pulse of a pulsed source. The latter can be effective in "freezing" the motion of an initially living sample. In addition, since damage processes are thought to take place on timescales related to the velocity of sound or slower, it appears that the image bearing signals resulting from fast-pulse illumination, could be away from the sample before any damage had time to occur. If this is indeed true it could provide a way to obtain information about the undamaged sample and a powerful way to study damage processes as well. With or without a subnanosecond pulse, the damage imnvolved in contact microscopy is considerable unless the sample is more radiation resistant than PMMA which is scarcely possible.

A significant variant of the contact method utilizes an electron optical imaging system instead of the resist detector. The latter makes an image using the photoelectrons emitted from a foil in contact with the x-ray-illuminated sample. A system of this kind, developed by F. Polack and colleagues [62] at Orsay, has already achieved a resolution of 0.3 microns.

The best performance achieved by contact methods is around 200 - 300 Å resolution, but difficulties with quantitative readout persist. The technique has been used a good deal with pulsed sources and is convenient for use with a wet cell and with a horizontal sample mounting stage. Considering how simple the technology is, it would certainly pay off handsomely if the remaining obstacles to faithful development and readout could be overcome.

THE ZONE PLATE IMAGING MICROSCOPE

The optics of this method are very similar to those of the visible light microscope and and are shown in fig 6. The most successful implementation of it is by G. Schmahl, D. Rudolf, B. Neimann and colleagues at the University of Gottingen who have developed their instrument [63] over a period of years, first at the ACO storage ring in Orsay and then at the BESSY facility in Berlin. The optical system begins with a large condenser lens (zone plate) which is set to image at less than its diffraction limited resolution and condenses the beam on to a pinhole. Since the focal length varies like $1/\lambda$, the zone plate-plus-pinhole amounts to a monochromator as well as a condenser. The sample is placed in or near the pinhole and is illuminated with the partially coherent beam. Spatial coherence is not needed for this system because EACH ELEMENT of the sample becomes a source of secondary scattered wavelets which coherently illuminate a small "microzone plate". The system gives a diffraction limited image with magnification which is variable in the range of about 50 to 300. This magnification is sufficient to make a recording on a lower resolution detector such as film or a solid state imager. Fig 8 is an example of a picture made using the microscope at BESSY by Vladimirsky, Kern, Meyer-Ilse and Attwood [64].

For best performance the making of the zone plates, particularly the resolution-determining microzone plate, requires the most advanced technology available. The Gottingen group has used two different strategies for this. The first is based on ultra violet holography [63] using deliberately aberrated wavefronts to allow for the recording of the zone plate (hologram) at the UV wavelength and the formation of the holographic image at x-ray wavelengths. This method was so successful that the group were able to demonstrate an image resolution of 550 Å, a figure which must be compared to the theoretical limit of 514 Å[65] for this method of manufacture using laser light of wavelength 2570 Å.

The second method of zone plate manufacture (implemented by the Gottingen group via a collaborative program with the University of Aachen) is electron beam writing [66]. Since this method is based on a programmable electron beam system, it has full flexibility in writing zone plates of various sizes and outer zone widths for use at a wide variety of x-ray wavelengths and focal lengths. The technology of electron beam writing of zone plates is widely used in the x-ray imaging community and is a matter of key importance for the developement of x-ray microscopy. We will give some general information on present achievements and future prospects, but a serious treatment of the subject is outside the scope of this article.

Electron beam writing of zone plates is being practiced currently in at least half a dozen countries. The most popular method is to write in resist but the group in Kings College London have chosen to use contamination writing [68], an approach which is more suited to implementation using commercially available electron microscopes. The most advanced programs are now delivering usable zone plates with 400-500 Å outer zone widths and therefore diffraction limited resolution values only slightly greater than this [64,66]. Several fabricators have also produced, or are working on, "experimental" zone plates with outer zone widths around 200 Å. These latter are usually of less good quality than the coarser ones but are an indication that viable 200 Å zone plates are likely to be available soon. Although PMMA, with its resolution limit of about 100 Å, or other lower resolution resists are used in all these methods, the contamination writing approach is less dependent on resist than the others; and there has recently been a significant proposal from the Kings College group for a PMMA-free, zone-plate-making procedure [69].

Returning to the subject of the imagimg microscope, we note that an important advantage of this scheme is its ability to use a spatially incoherent x-ray beam. This, coupled with the related capability for imaging all sample elements in parallel, translates into very fast imaging, even with a storage ring bending magnet source. With such a source at BESSY the exposure times with typical beam currents are in the range 10-100 sec. The recognized disadvantage of the imaging geometry is the unnecessary dose that the sample must receive to make up for the inefficiencies of the zone plate and detector which occur AFTER the sample. At present these two devices have a combined efficiency of around 1% which implies 100 times more dose to the sample than for an ideal syatem. However, there are two things to be said about this. Firstly, there are ways to improve the efficiencies of the zone plate and detector and some of these are already in hand. Secondly, it may turn out for some biological applications that if the image can be made fast enough then the dose is of secondary importance. How fast is fast enough? will be a matter for individual cases but the imaging microscope is well adapted for fast imaging and could no doubt be made to go faster than the BESSY speed using a third-generation, synchrotron, x-ray source or even an undulator on a second generation one.

SCANNED IMAGE ZONE PLATE MICROSCOPY

In order to address the damage problem, one would like to position the zone plate and its losses before the sample and have a detector with a nominal efficiency of 100%. These conditions are achieved by the scanning geometry illustrated in fig 9. The zone plate focusses the beam to a diffraction-limited spot (ie a single-mode beam is used) and the sample is scanned through

the spot in a raster pattern using high resolution piezoelectric transducers. At each dwell position the x-rays transmitted through the sample are counted using a flow proportional counter which is close to 100% efficient in the soft x-ray region. An example of a picture [70] made in this way by S-F. Fan, H. Rarback, H. Ade and J. Kirz at the Brookhaven microscope is shown in fig 10.

Additional advantages of this scheme are the convenience with which the data can be stored and manipulated by the computer, the fact that the sample can be conveniently kept in atmospheric pressure air or helium and the natural way the system includes absorption microanalysis [51] as one of its operating modes. Against these considerations is the requirement for an x-ray beam with full spatial coherence and the serial nature of the data-taking. Both of these factors tend to prolong the exposure times which, at Brookhaven, are currently 1-2 minutes for a high resolution, 256x256-element picture using an undulator. There are still prospects for a significant improvement using existing sources and exposures of small fractions of a second are projected using a third generation source such as the ALS.

Scanning x-ray microscopes using zone plate lenses are now being operated at Brookhaven [71] by a consortium including The National Sychrotron Light Source, The State University of New York at Stony Brook, Lawrence Berkeley Laboratory and IBM, at Daresbury [72] by researchers from Daresbury and Kings College London and at BESSY [73] by the Gottingen group. Still others are under developement. In keeping with the state-of-the-art of zone plate fabrication mentioned earlier, these groups are achieving resolution values in the region of 500 Å with prospects of improvement to 200 Å reasonably soon and 100 Å ultimately. To achieve resolution below 100 Å will need a new "resist-free" method of making zone plates. Such a method might be based on contamination writing, as noted above, or on the so-called "jelly roll" technique being studied by the Gottingen group [63].

As we have seen, the standard scanning x-ray microscope using absorption contrast is best used in the water window wavelength region. In this case, state-of-the-art pictures can be obtained with a dose of about 1 Mrad for a biological sample around one micron thick. However, the potential of the instrument is not limited to this mode of operation. As noted earlier, it should be possible to obtain phase contrast using a split detector [32] and thereby make biological images at higher photon energies with dose values not very different than those prevailing in the water window. The limitation on the photon energy in this case would be the capability of operating a zone plate or phase plate which, with some compromise of resolution extends the range up to at least 4keV [38].

X-RAY HOLOGRAPHY

Although the majority of x-ray imaging experiments today use one of the three techniques described above, it is also possible to obtain sample information by exploitation of the diffracted field as is done in crystallography. To do this one must have a method for determining and using both the amplitudes and phases of the diffracted wave. In the soft x-ray region, holography provides one such method. An alternative approach would be to measure only the intensity of the diffracted field and use computational methods to infer the phases. D. Sayre [74] has made considerable progress in demonstrating that both the recording and calculation steps of such a program can, in fact, be accomplished.

It was in 1948 that D. Gabor [75] first pointed out that it is possible to record both the amplitude AND phase of a wave using an intensity detector provided a suitably coherent phase reference wave is available to beat against the signal wave. There is a long history, beginning in the early 1950s, of attempts to make such "hologram" recordings using x-ray tube sources and photographic film detectors. The hope was that one would be able to record the hologram with x-rays and reconstruct it with visible light thereby achieving a three-dimensional "microscope" with resolution superior to the light microscope and without the need to fabricate a lens with such resolution.

These hopes were never realized. Holograms of reconstructible quality [76] were obtained in relatively few cases and none gave images with resolution higher than the light microscope. As a result x-ray holography became a dormant field by the mid 1970's.

This general failure can be understood in terms of the poor coherence properties of the x-ray tube sources and the low resolution of the photographic film detectors that were used. The use of an undulator source and a resist detector makes it possible to record holograms with reasonable exposure times and much finer fringe detail than the earlier workers achieved. Such holograms are now being made in France, Japan and the United States. In all these cases, the chosen holographic geometry was the Gabor, in-line configuration (fig 11).

The French group D. Joyeux, S. Lowenthal, F. Polack and A. Bernstein, [77] are based at the Institut d'Optique and the Laboratoire de L'Utilisation de Rayonnement Electromagnetique (LURE) and have used an undulator on the ACO storage ring to make phase holograms of diatoms and other objects on preexposed resist. They have chosen a laser-based approach to reconstruction that uses sophisticated optical correction methods to deal with aberrations. The procedure is optimized with regard to speed, convenience, linearity and signal-to-noise rather than resolution. One anticipates further improvements in the performance of this scheme when the program transfers to the new SUPERACO storage ring.

The group in Japan is using an undulator on the PHOTON FACTORY storage ring in a natural continuation of the earlier work of S. Aoki, S. Kikuta and collaborators, who achieved the most successful holograms of the 1970's. The experiments [78] are in an early phase but recent improvements to the storage ring have made it a highly suitable source for the continuation of this widely admired holography program.

A group comprising C. Jacobsen, J. Kirz, S. Rothman and the present author have been making holograms using the National Synchrotron Light Source soft x-ray undulator beamline [79], which was used to provide a spatially and temporally coherent beam of 25 Å x-rays [47]. The optical layout of the beamline (fig 12) is similar to that needed in x-ray imaging experiments generally. For the hologram shown in fig 13 [47], the coherent flux was about 10^8 photons per second which gave about a one-hour exposure time and a dose of about 200 Mrads. The most recent recordings have exposure times of 2-4 minutes.

The recordings were made on 2000 Å thick layers of resist coated on 1200 Å thick silicon nitride windows supported on silicon frames. The developed resist was shadowed with gold-palladium at glancing incidence and imaged in the transmission electron microscope (TEM). The resulting photographic negative was finally digitized using a microdensitometer.

The analysis [80] takes advantage of the fact that all holograms can give

an aberration-free reconstruction if they are illuminated with the original reference wave. This would not be a useful thing to implement experimentally for an x-ray Gabor hologram because the reconstructed image would not be magnified. However, it is possible to mimic the same process in a computer and display the result to get any required magnification. The calculation really consists of numerically simulating the propagation of the reference wave from the hologram to the image in the Fresnel Approximation (ie taking the Fresnel Transform of the data). The algorithm for doing this involves multiplying the data entries by a quadratic phase factor and taking the Fast Fourier Transform. On a MicroVAX II computer, it takes about five minutes. The process of focussing takes place at this stage of the procedure and involves adjustment of the propagation distance.

An example of both a hologram and a reconstructed image from the Brookhaven experiment are shown in fig 13. The samples were mounted on electron microscope grids and by reconstructing the image of the edge of one of the grid bars, it was determined that the system resolution, defined as the distance from 10% to 90% of the step-height, was not worse than 630 Å. However, on the basis of spectral analysis of the hologram recordings, we can show that information was recorded at less than 200 Å resolution. This presents a challenge to improve the reconstruction technique. The resolution was influenced by the frequency at which the hologram was sampled, which caused a loss of higher frequency information. Therefore, it is not legitimate to infer anything about general dose requirements from the dose used in this case.

As one might expect, there are considerable hopes for using lasers in the making of x-ray holograms [96,97,98,99]. The first step in this approach has been made by Trebes et al. [100] who used the Lawrence Livermore Laboratory 206 Å laser to record and reconstruct holograms of test objects at a resolution of 5 microns.

THREE-DIMENSIONAL IMAGING

One of the main goals of imaging by holography or D. Sayre's diffraction procedure, is to provide three-dimensional information. The diffraction limits to this depend on the NA as described above. The NA in holography is not normally defined by the size of a physical aperture such as the edge of a lens but is determined in a complex way by the transfer function of the resist as a function of frequency (aperture angle), the power spectrum of the sample and the coherent x-ray exposure. These parameters, together, determine the roll-off of the signal-to-noise ratio at high frequencies and hence the NA and the resolution.

The transverse and longitudinal resolutions are related through the numerical aperture (equations 1, 5) and for experiments at low transverse resolution (low NA) the longitudinal resolution may be much larger than the sample thickness making the measurement two-dimensional. (Note that for this two-dimensional imaging regime, the dose scales as the SQUARE of the resolution.) To achieve three-dimensional imaging one has therefore to improve the numerical aperture and thus both types of resolution. For example, the Brookhaven holography experiments reported above had a numerical aperture of about 1/40. If that could be improved to about 1/8 then we would have a transverse resolution of 100 Å and a longitudinal one of 1600 Å, which would be quite useful. However, once true, three-dimensional imaging was being

practiced, the dose required would scale as the SIXTH POWER of the transverse resolution (see later), so progressing toward 100 Å would certainly imply that one would be dealing with extraordinarily high doses and it is hard to imagine making more than a few exposures of a sample (say two for a stereo-pair, for example) if one pushed to the limit in that way.

Another approach may be exemplified as follows. Suppose we have an exposure at some given resolution and that we have a way to improve that by a factor of two for a hologram from a single view direction. This would give four times better depth resolution and sixty four times more dose. However, an alternative strategy would be to forego the factor two resolution improvement and make sixty four more exposures at the same resolution with different illumination directions. This would provide greatly superior three-dimensional mapping and would lead us into a form of tomography which is usually called diffraction tomography [81,82] because the wavefield emerging from the sample spreads out and propagates according to the laws of diffraction. This is in contradistinction to the conditions normally encountered in computerised axial tomography (CAT) scanning, which is based on the laws of geometrical optics.

The two choices discussed here represent opportunities to seek either the best resolution or the best three-dimensionality. We suggest that resolution is not the only criterion for useful imaging and that the advantage of being able to measure the full three-dimensional density map,(or other type of information such as chemical), may justify some compromise of the resolution.

The choice between the two approaches is partly an instrumental one. If the available source was an x-ray laser, then the large dose, single shot approach would be required. With a synchrotron radiation source the diffraction tomography option would be somewhat more compelling.

In the next section we review some of the basic ideas of diffraction tomography and provide some references where further information can be found.

DIFFRACTION TOMOGRAPHY

A diffraction tomography experiment could consist of illuminating the sample with monochromatic plane waves and measuring both the amplitude and phase of the diffracted field at some plane perpendicular to the illuminating direction and downstream of the sample. The same experiment would then be repeated many times for different illumination directions. Starting from an understanding of CAT scanning one might suppose that by allowing the wave to spread and diffract, the information content would be compromised severly. However, it was shown by Wolf in 1969 [83] that the information may in fact be preserved and can be extracted by taking the complex two-dimensional Fourier Transform of the measured wavefield (see equation (9) and discussion). Provided the measured wavefield is the same as the Born Approximation to the wavefield, this determines certain values of the three-dimensional Fourier Transform of the complex refractive index distribution of the scattering object at Fourier frequencies lying on the Ewald Sphere in frequency space. This is known as the Generalised Projection Slice Theorem. By making further measurements at different illumination directions one can fill in more data points on other Ewald Spheres that are rotated about the origin with respect to the first one. When a sufficient number of spheres of data have been accumulated, one strategy is to interpolate the data to fill the frequency space on an appropriate grid of points. A three-dimensional Fourier Transform

then returns the desired values of the complex refractive index distribution of the sample.

This procedure has been applied using sound, radio waves, microwaves and seismic waves, but not, so far as we know, x-rays, presumably due to the difficulty in obtaining the phases in this case. The computational methods that can be used are not limited to those based on interpolation and the Generalised Projection Slice Theorem as described above. A good deal of effort has been devoted to designing very general and powerful algorithms [81,82] which deal with limited amounts of data and noisy data and which allow prior knowledge to be used. We are interested in understanding the conditions under which this kind of approach could work with soft x-rays. At first sight it seems that the whole procedure depends on the use of the Born Approximation. However, cases where the Born Approximation breaks down can be treated by a device called the Rytov Approximation. [82,84,85]. This method essentially provides an approximate way to calculate what the Born Approximation to the scattered field WOULD have been, had you done a direct, forward calculation using it. From the point of view of implementation the Rytov method involves virtually the same amount of processing as the Born.

In Table II we provide some optical data for biological materials at 30 Å which allow one to get a feeling for whether the Born and Rytov validity criteria are met in soft x-ray imaging experiments. The criteria for both are based on the idea of a linear approximation to the wave equation for "weak" scattering of the incident wave. (The exact calculation is very intractable and little progress has been made with it.) Both approximations usually require that the scattering potential (the refractive index distribution) should be expressible as the sum of a background term that is real and a sample term that may be complex but must be small compared to the background. This is well satisfied in our case because the refractive index is always equal to unity minus small correction terms. Both also require that the scattered amplitude be small compared to the incident. This is also likely to be true for all soft x-ray diffraction experiments. The essence of the Born Approximation is that each element of the sample is assumed to be illuminated with the UNMODIFIED incident wave. This requires that the total attenuation be small as well as the scattering and this is certainly not satisfied by most soft x-ray imaging experiments. It is this difficulty that is resolved by the Rytov Approximation because it requires only that the attenuation and phase change PER WAVELENGTH [84,85] should be small. This is a much easier requirement and as shown in the table is well satisfied for the kind of experiments that we envision.

The conclusion from this is that soft x-ray imaging experiments in or near the water-window spectral range (23-44 Å) do indeed satisfy the conditions for the use of the established procedures of diffraction tomography using the Rytov Approximation. This opens possibilities for new types of experiments in the future.

TABLE II

OPTICAL PROPERTIES OF BIOLOGICAL MATERIALS [96] AT 30 Å

PROPERTY	WATER	PROTEIN	DNA	LIPID	CARBOHYDRATE
Index real part (δ).	0010	.0015	.0017	.0012	.0017
Index imag part (β)	.000047	.00057	.00076	.00038	.00039
Phase change per wavelength ($2\pi\delta$) (Radians)	.0063	.0094	.011	.0078	.011
Attenuation per wavelength ($4\pi\beta$)	.00059	.0072	.0095	.0048	.0049
Absorption length (microns)	5.1	.42	.32	.36	.61
phase change per abs. length ($\delta/2\beta$) (radians)	10.7 (2.1 per micron)	1.3	1.1	1.62	.2

RADIATION DAMAGE

There is very little experimental evidence available concerning the effect of soft x-rays on biological material. What we would like to understand is the degradation of the image that we measure AT THE RESOLUTION THAT WE ARE USING and in the context of what we hoped to learn from the image. In the absence of direct evidence on this point we must turn to the evidence available from other imaging methods particularly x-ray crystallography and electron microscopy coupled with our understanding of the physics of the interaction of soft x-rays with matter.

The x-ray crystallography community have been illuminating protein crystals with x-rays for something in excess of half a century. However, in spite of this extensive experience, quantitative data on radiation damage is quite hard to find. The broad conclusion seems to be [86] that to obtain a usable data set, one has to apply a radiation dose of at least 1-10 Megarads and that protein crystals in general are able to withstand such a dose and still provide 1.5-2.0 Å resolution data, particularly if the dose is applied sufficiently rapidly.

For electron microscopy, values of the critical radiation dose for damage to various organic materials are tabulated in the reviews by Glaeser and Reimer [87,88]. The average value is about 0.01 Coulombs/cm^2 with a variation of around one order of magnitude in either direction for the range of materials that were measured. At 60 keV this is equivalent to 1000 Megarads. The end-points defining the critical dose in the above measurements were mostly loss of electron diffraction efficiency and mass loss.

From a microscopy viewpoint the most useful form of radiation damage

measurement is that in which the fading of particular diffraction spots is measured as a function of dose [89,90,91]. From the d-spacing of the corresponding Bragg planes one can tell the resolution level at which detail is being destroyed. Glaeser and Taylor [90] observed that, in their experiments on crystals of the enzyme catalase, the resolution level decreased linearly with the logarithm of the applied dose. Their curves allow an extrapolation to the resolution values that one would like to use in x-ray imaging experiments and thus an estimate of the permitted dose in those cases. Values of the dose to destroy 100 Å structural detail are between $2x10^9$ and $1x10^{10}$ rads for the various preparations used. However, all the preparations were either embedded or frozen so that the enzyme molecules were at least partially protected by the "cage" effect from attack by the products of the radiolysis of water. In aqueous solution one would expect the material to be rather more radiation sensitive but it is not clear on what timescale the damaging processes would work. It is known from the increased radiation tolerance of protein crystals at synchrotron radiation facilities (high dose rate) compared to laboratory sources (low dose rate) that some of the damage mechanisms are slow, requiring at least minutes to operate. It would be valuable to have a better understanding of this matter.

It is important to recognize that the levels of dose that we are discussing are far in excess of the levels where major biological changes occur. However, we also note that this has not prevented electron microscopists and x-ray crystallographers from making outstanding contributions to biological science. In fact, important biological effects occur at the doses needed for imaging by all of the techniques mentioned so far including the x-ray ones. The reason that x-ray microscopy promises to provide some progress in the imaging of radiation sensitive samples is not that x-rays deliver any less dose per particle, but rather that the lower background and improved contrast of x-ray images lead to a higher quality of information for whatever dose is permitted.

There are also various ways to reduce radiation damage (cooling, radical scavengers etc.) that are used by some experimenters, and of course these could also be applied to the x-ray techniques discussed here.

Now that we have discussed the nature of the contrast and the physical processes involved in forming images in the four types of microscopes under consideration, we are in a position to calculate the radiation doses involved. Such calculations have already been done by Sayre et al [93] for a number of cases including x-ray amplitude contrast and some comparative studies of illumination by electrons but not for x-ray phase or scattering contrast. Calculations of the dose required for holographically imaging spherical objects have been made by London et al. [101].

Following Glaeser [87], Kirz et al., [35] Sayre et al. [93] and others, we choose to adopt the so-called Rose criterion [92] for detectability. This states that for our definition of contrast, a feature will be detectable if the contrast is at least five times the noise-to-signal ratio. If the noise is shot noise, this implies that the required number of counts N, is given by

$$C = 5\ \Delta N/N$$

or

$$N = 25/C^2 \qquad (34)$$

We will calculate the dose applied in obtaining N counts from a given sample

pixel. We do not include any allowance for imperfect recording of the counts or for achieving an image quality higher than the minimal detectability implied by the Rose criterion. Furthermore, our definition of contrast is very simplistic (more so than that used in [93]) because for two-dimensional samples, we consider equal amounts (thicknesses) of the interesting material and the background. If the interesting material had a thickness less than the background or a density less than 100%, then the phase or amplitude contrast would be reduced, say by a fraction f. This would lead to an increase by a factor f^{-2} in N and hence also in the dose.

We are seeking to understand the influence of the intrinsic material properties of the sample on the doses involved in x-ray imaging. In light of this, we make NO allowance for particular experimental imperfections.

We consider the same three examples of contrast mechanisms that we used earlier, namely, amplitude, phase and scattering for the same two materials, protein (of density ρ) and a background of water. The first two are assumed to be used with a two-dimensional sample of thickness t and in all cases the transverse resolution is taken to be d. The dose is the energy deposited per unit mass.

For amplitude contrast, the dose (for given N and d) is inversely proportional to the thickness so we calculate the dose-thickness product D.t

$$D_a t = (N/\rho)(1/d^2) \tag{35}$$

For phase contrast we get

$$D_p = (2r_o hc)(aN/\rho)(1/d^2) \tag{36}$$

For scattering contrast our task is more complicated because the scattering (leading to imaging) and the absorption (leading to dose), scale differently with pixel size. In order for N x-rays to be scattered by the pixel, $N\sigma_a/\sigma_s$ will be absorbed. Using (20) we arrive at the following expression for the dose associated with scattering contrast.

$$D_s = (2hc/\pi/r_o)(aN/\rho/s_{pw}{}^2)(1/d^6) \tag{37}$$

In all three expressions, we have kept the fundamental constants, the material-dependant factors and the resolution dependence separate.

As an example of the use of these equations we show in fig 14, the dose (or the dose-thickness product) required under the assumptions given, to image a feature of transverse width, 200 Å. The most striking features of all of the curves are the regions where the required dose diverges due to the contrast passing through zeroes near the sulfur L and carbon K edges. More encouraging is the behavior of the the amplitude (absorption) contrast which is quite expected and shows, once again, the value of the water window in providing a natural contrast between protein and water. It is less welcome to see that the amplitude contrast is so low (fig 5) at higher energies that the dose increases more than two orders of magnitude compared to the water window. Unfortunately this applies to the region of the K edges of such biologically important elements as sulfur, phosphorus, chlorine, potassium and calcium. However, what amplitude contrast cannot do, the other two contrast mechanisms

seem well suited to do.

The phase and scattering contrast curves are rather similar in shape because the scattering strength tends to be dominated by f_1 in much of the spectral region. For both of them, the region near to the oxygen edge is interesting for imaging although above the energy of the oxygen edge there are also excellent opportunities. The advantage that these forms of contrast hold over absorption contrast outside the water window is that D_p and D_s contain the absorption strength explicitly while Da does not. Thus D_p and D_s profit from the rapid (-5/2 power) falloff of f_2 with energy well above the K edges of the light elements, while D_a gains nothing because in absorbtion contrast one must always continue to absorb!

ACKNOWLEDGEMENTS

The author wishes to acknowledge invaluable continuing discussions with R. Glaeser, C. Jacobsen, J. Kirz, S. Rothman and D. Sayre. This work was supported by the Director, Office of Energy Research, Office of Basic Energy Sciences, Material Sciences Division, of the U.S. Department of Energy under Contract DE-AC03-76SF00098. Some of the work reported was carried out at the National Synchrotron Light Source at Brookhaven National Laboratory which is similarly supported by the Department of Energy under Contract DE-AC02-76CH00016.

FIGURE CAPTIONS

1. Comparison of the penetration of soft x-rays and electrons in water and protein in the spectral regions in which they are often used for imaging. Data are taken from [93,96].
2. Notation for the mathematical description of scattering of the incoming x-ray wave by the sample.
3. Geometry of the Ewald sphere relative to the in and out directions of the x-rays and the optical aperture. The NA is sin ϕ in this case.
4. Plot of scattering strength of water, protein and protein against a background of water. The protein-water difference signal in the latter case is calculated by means of a coherent subtraction.
5. Contrast (C) between protein and water according to the definitions given in equations 24, 25, 26. Note that to allow use of a logarithmic scale the quantity plotted is actually 1+C so that the line "y=1" represents zero contrast.
6. Optical layout of the Gottingen, imaging x-ray microscope including the π-by-two phase shifter that produces Zernike phase contrast.
7. Comparative brightness plot for various x-ray sources from K. J. Kim [43].
8. Example of a picture made with the Gottingen, imaging microscope by Vladimirsky, Kern, Meyer-Ilse and Attwood [64]. The image is a part of a larger picture of the gate level pattern of an experimental 0.1 micron metal-oxide-semiconductor field-effect transistor. The marked feature is a clearly resolved 700 Å gap.
9. Optical layout of a scanning x-ray microscope showing the geometry of x-ray illumination. The zone plate itself forms the aperture which rejects all radiation except that in a single mode as explained in the text.
10. Image of shrimp muscle as described in reference [70] made using the

Brookhaven microscope by S-F. Fan, H. Rarback, H. Ade and J. Kirz

11. Geometry for recording Gabor holograms such as that in fig 13 (top) and geometry that could be used to make Fourier holograms using a zone plate lens (bottom).
12. Optical layout used in recording the hologram in fig 13 at the National Synchrotron Light Source X-ray ring at Brookhaven National Laboratory.
13. Hologram and reconstruction of a clump of air dried zymogen granules taken from the pancreatic acinar cell of a fasted rat.
14. Plots of calculated dose required to image a resolution element consisting of protein immersed in water based on the assumptions given in the text and on the diagram. Note that the curve for amplitude contrast is for the dose-thickness product in Mrad.microns.

REFERENCES

1. D. Gabor in preface to L. Marton, "Early History of the Electron Microscope", San Francisco Press, 1968.
2. D. F. Parsons (ed), Conference on "Short Wavelength Microscopy", Ann. N. Y. Acad. Sci., 306 (1978)
3. D. F. Parsons (ed), Conference on "Ultrasoft x-ray microscopy: its Application to biological and Physical Sciences", Ann. N. Y. Acad. Sci. 342 (1980).
4. G. Schmahl and D. Rudolf (eds), "X-ray Microscopy", Proceedings of a conference at Gottingen, Springer Verlag, Berlin, 1984.
5. P. C. Cheng, G-J. Jan (eds) "X-ray Microscopy, Instrumentation and Biological Applications", proceedings of a conference in Taipei, Taiwan, Springer Verlag, Berlin, 1986.
6. D. Sayre, M. R. Howells, J. Kirz, H. Rarback (eds), "X-ray Microscopy II", proceedings of a conference at Brookhaven National Laboratory, Springer Verlag, 1988.
7. J. Kirz, D. Sayre, "Soft X-ray Microscopy of Biological Specimens", in "Synchrotron Radiation Research", H. Winnick and S. Donniach (eds), Plenum, New York, 1980.
8. J. Kirz and H. Rarback, Rev. Sci. Instrum. 56, 1 (1985).
9. M. Howells, J. Kirz, D. Sayre, and G. Schmahl, "Soft x-ray microscopes", Physics Today, August 1985, 2-11.
10. There is a series of conferences entitled X-ray Optics and Microanalysis and similar titles which began in 1956 and has continued at three year intervals until the present. Originally these had valuable material on x-ray microscopy but this diminished after about 1970. The first five were at location (editor, publisher) as follows: 1956 Cambridge (V. E. Cosslett, A. Engstrome, H. H. Pattee, Academic), 1959 Stockholm (A. Engstrome, V. E. Cosslett, H. H. Pattee, Elsevier), 1962 Stanford (H. H. Pattee, V. E. Cosslett, A. Engstrome, Academic), 1965 Orsay (R. Castaing, P. Deschamps, J. Philibert, Herman), 1968 Tubingen (G. Molenstedt, K. H. Gaukler, Springer Verlag)
11. V. E. Cosslett, W. C. Nixon, "X-ray Microscopy", Cambridge, 1960. See section 11.13 for information on the commercial production of the projection x-ray microscope.
12. P. C. Cheng, D. M. Shinozaki, K. H. Tan, op. cit. ref 5, P. C. Cheng et al. in "Examining the Submicron World", R. Feder, J. W. McGowan, D. Shinozaki (eds), Plenum, New York 1984 and R. Feder et al Science,

227, 63 (1985).
13. Reference 11 and references therein are excellent sources on the history of the x-ray microscope. For additional material see S. P. Newberry in "X-ray Microscopy Instrumentation and Biological Applications", p. 346, op.cit. ref 5 and for holographic microscopy see C. Jacobsen, Proceedings of the Tochigi Conference on X-ray Microscopy, August, 1988, to be published.
14. G. J. Burch, Nature, Lond. 54, 111 (1896) and F. Ranwez, C. R. Acad. Sci. Paris, 122, 841 (1896), see also T. A. Hall, H. O. E. Rockert, R. L. deC. H. Saunders, "X-ray Microscopy in Clinical and Experimental Medicine", Charles C. Thomas, Springfield Illinois, 1972.
15. P. Kirkpatrick, A. V. Baez, J. Opt. Soc. Am. 38,776 (1948).
16. V. E. Cosslett, W. C. Nixon, Nature, Lond. 168, 24 (1951), Proc. Roy. Soc. B, 140, 422 (1952).
17. S. P. Newberry, in "X-ray Microscopy Instrumentation and Biological Applications", page 126, op. cit. ref 5.
18. R. W. James, "The optical principles of the diffraction of x-rays", Oxbow, Woodridge, CT, 1982.
19. M. Born, E. Wolf, "Principles of Optics", Pergamon, Oxford, 1980.
20. N. F. Mott, H. S. W. Massey, "The theory of atomic collisions", 2nd ed. Oxford, 1949, para 4, chap VI.
21. J. W. Goodman, "An introduction to Fourier optics", MacGraw-Hill, San Francisco, 1968.
22. B. L. Henke, P. Lee, T. J. Tanaka, R. L. Shimabukuro, B. K. Fujikawa, Atomic Data and Nuclear Data Tables, 27, 1 (1982) and B. L. Henke, J. C. Davis, E. M. Gullikson, R. C. C. Perera, Lawrence Berkeley Laboratory report, LBL-26259 UC-411.
23. F. Wooten, "Optical properties of solids", Academic, New York, 1972 and R. N. Bracewell, The Fourier Transform and its applications", McGraw-Hill, New York, 1978.
24. W. Heitler, "The quantum theory of radiation", 3rd edition, Dover, 1984, para 21 eq 14. plus our eq 13.
25. E. F. Plechaty, D. E. Cullen, R. J. Howerton, "Tables and graphs of photon interaction crossections from 0.1 keV to 100 MeV", Lawrence Livermore Laboratory report UCRL-50400, vol 6, rev 3.
26. M. R. Howells, in "X-ray Microscopy II", op. cit. ref 6. Treatment of the Thomson scattering process used in this reference can be found, for example, in J. D. Jackson, "Classical Electrodynamics", Wiley, New York, 1967.
27. F. Zernike, Z. Tech. Phys. 16, 454 (1935).
28. J. Kirz, J. Opt. Soc. Am. 64, 301 (1974).
29. G. Schmahl, D. Rudolf, op. cit. ref 5.
30. P. K. Mondal, S. Slansky, Appl. Opt. 9, 1879 (1970).
31. T. Wilson and C. J. R. Sheppard, Optik, 59, 19 (1981).
32. D. K. Hamilton, Tony Wilson, Appl. Opt. 23, 348 (1984).
33. G. Schmahl, D. Rudolf, P. Guttman, op. cit. ref 6.
34. G. Nyakatura et al op. cit. ref 6.
35. J. Kirz, D. Sayre, J. Dilger, Ann. NY. Acad. Sci. 306, 291 (1978).
36. J. Kirz, in "Scanning Electron Microscopy II", SEM Inc., Chicargo, 1980.
37. J. Kirz, Ann. NY. Acad. Sci. 342, 273 (1980).
38. M. R. Howells, J. Kirz, D. Sayre, section II-29 in "Report of the Workshop on the Scientific case of a 6-GeV Synchrotron Source", K. O.

Hodgson, J. B. Cohen (eds), Argonne National Laboratory, 1985.
39. C. J. Sparks, Jr. in Synchrotron Radiation Research, H. Winnick, S. Doniach (eds), Plenum, New York, 1980.
40. D. L. Mathews et al, Phys. Rev. Lett. 54, 110 (1985) and M. D. Rosen et al., Phys. Rev. Lett. 54, 106 (1985).
41. S. Suckewer, C. H. Skinner, D. Kim, E. Valeo, D. Voorhees, A. Wouters Phys. Rev. Lett. 57, 1004 (1986).
42. D. Attwood, K. Halbach, K. Kim, Science, 228:1265-1272, 1985.
43. K. J. Kim in "X-ray Data Booklet", Lawrence Berkeley Laboratory publication PUB-490.
44. P. C. Cheng, D. M. Shinozaki, K. H. Tan, in "X-ray Microscopy, Instrumentation and biological applications", op. cit ref. 5.
45. D. Rudolph, B. Niemann, G. Schmahl, O. Christ, in "X-ray microscopy", op. cit ref. 4.
46. P. Horowitz, J. A. Howell, Science, 178, 608 (1972), B. Niemann, Proc. SPIE 733, 422 (1986), H. Rarback, J. Kenney, J. Kirz, X. S. Xie, in "Scanned Image Microscopy", Academic, London, 1980.
47. M. Howells, C. Jacobsen, J. Kirz, R. Feder, K. McQuaid, S. Rothman, Science, 238, 514 (1987).
48. K. L. D'Amico, H. W. Deckman, B. P. Flannery, W. G. Roberge, in "X-ray Microscopy II" op. cit. ref. 6.
49. J. H. Underwood, A. C. Thompson, Y. Wu, R. D. Giauque, Nucl. Inst. Meth. A266, 296 (1988).
50. L. Jochum in "X-ray Microscopy II", op. cit. ref. 6.
51. C. Jacobsen et al. Phys. Med. Biol. 32, 431 (1987).
52. I. Haller, M. Hatzakis, R. Srinivasan, IBM J. Res. Devel. 12, 251,1968.
53. E. Spiller, R. Feder, in "X-ray Optics", H.-J. Queisser (ed), Springer Verlag, Berlin, 1977.
54. R. Feder, V. Mayne-Banton in "Examining the Submicron World", op. cit. ref. 12.
55. W. A. Ladd, W. M. Hess, M. W. Ladd, Science, 123, 370 (1956).
56. R. Feder, D. Sayre, E. Spiller, J. Topalian, J. Kirz, J. Appl. Phys. 47, 1192 (1976).
57. E. Spiller, R. Feder, J. Topalian, D. Eastman, W. Gudat, D. Sayre, Science 191, 1172 (1976).
58. J. Pawlak, P. C. Cheng, D. M. Shinozaki in "X-ray Microscopy Instrumentation and Biological Applications", op. cit. ref. 5.
59. D. M. Shinozaki, B. W. Robertson in "X-ray Microscopy Instrumentation and Biological Applications", op. cit. ref. 5.
60. K. Shinohara et al, Photochem. Photobiol. 44, 401 (1986).
61. C. Jacobsen, D. Abrahams, private communication.
62. F. Polack, S. Lowenthal, D. Phalippou, P. Fournet in "X-ray MicroscopyII", op. cit. ref. 6.
63. G. Schmahl, D. Rudolf, B. Niemann in "Uses of Synchrotron Radiation in Biology", H. B. Stuhrmann (ed), Academic, London, 1982.
64. Y. Vladimirsky, D. Kern, W. Meyer-Ilse, D. Attwood, J. Phys. Lett. 54, 286 (1989).
65. P. Guttman in "X-ray Microscopy", op. cit. ref. 4.
66. V. Bogli et al in "X-ray Microscopy II", op. cit. ref. 6.
67. A. N. Broers, M. Hatzakis, Scientific American, 227, 227 (Nov 1972).
68. C. Buckley et al. in "X-ray Microscopy II", C. Buckley, Ph.D. thesis, Kings College London, 1987, and A. G. Michette "Optical Systems for

Soft X-rays", Plenum, London, 1986.
69. A. G. Michette, C. J. Buckley, Proc. SPIE volume 1140, to be published.
70. S-F. Fan, H. Rarback, H. Ade, J. Kirz in "X-ray Microscopy II", op. cit. ref. 6.
71. H. Rarback et al Rev. Sci Instrum. 59, 52 (1988).
72. G. R. Morrison, Proc. SPIE volume 1140, to be published.
73. B. Niemann in "X-ray Microscopy II", op. cit. ref. 6.
74. B. Sayre, R. P. Haelbich in "X-ray Microscopy", op. cit. ref. 4, D. Sayre, W. B. Yun, J. Kirz in "X-ray Microscopy II", op. cit. ref. 6, D. Sayre in "X-ray Microscopy Instrumentation and Biological Applications", op. cit., ref. 5.
75. D. Gabor, Nature, 161, 777 (1948).
76. S. Aoki, Y. Ichahara, S. Kikuta, Jpn. J. Appl. Phys. 11, 1857 (1972), S. Aoki, S, Kikuta, Jpn. J. Appl. Phys. 13, 1385 (1974).
77. D. Joyeux, S. Lowenthal, F. Polack, A. Bernstein in "X-ray Microscopy II", op. cit. ref. 6, D. Joyeux, F. Polack, Proceedings of the OSA Topical Meeting "Short Wavelength Coherent Radiation: Generation and Applications", Cape Cod, 1988. To be published in American Institute of Physics Conference Proceedings series.
78. S. Aoki, S. Kikuta in "Short Wavelength coherent Radiation: Generation and Applications", American Institute of Physics Conference Proceedings No. 147, 1986.
79. H. Rarback, C. Jacobsen, J. Kirz, I. Mcnulty, Nucl. Inst. Meth. A266, 96 (1988).
80. C. Jacobsen, J. Kirz, M. R. Howells, S. Rothman, European J. Cell Biol, Suppl. 25, vol. 48, 177 (1989), C. Jacobsen, M. Howells, J. J. Kirz, K. McQuaid, S. Rothman, Cape Cod Conference, op. cit. ref. 77.
81. A. C. Kak in "Array Signal Processing", S. Haykin (ed), Prentice-Hall, Englewood Cliffs, 1985.
82. A. J. Devaney, Inverse Problems 2, 161 (1981).
83. E. Wolf, Opt. Comm. 1, 153 (1969).
84. V. I. Tatarski, "Wave Propagation in a Turbulent Medium", McGraw-Hill New York, 1961
85. A. J. Devaney, Opt. Lett. 6, 374 (1981).
86. K. Moffat et al in "Biological Applications of X-ray Diffraction", H. D. Bartunic, B. Chance (eds), Academic, New York, 1986, T. L. Blundell, L. N. Johnson, "Protein Crystallography", Academic, 1976, J. R. Helliwell, Rep. Prog. Phys. 47, 1403 (1984), K. Moffat, E. Lattman, private communications.
87. R. Glaeser in "Physical Aspects of Electron Microscopy and Microbeam Analysis", B. M. Siegel, D. R. Beaman (eds), Wiley, New York, 1975.
88. L. Riemer, "Transmission Electron Microscopy", Springer Verlag, Berlin, 1984.
89. M. Isaacson, op. cit. ref. 87.
90. R. M. Glaeser, K. A. Taylor, J. Micr. 112, 127 (1978).
91. S. B. Hayward, R. M. Glaeser, Ultramicroscopy, 4, 201 (1979).
92. A. Rose, J. Soc. Motion Picture Engrs. 47, 243 (1946).
93. D. Sayre, J. Kirz, R. Feder, D. M. Kim, E. Spiller, Ultramicroscopy 2, 339 (1977).
94. E. Spiller in "Handbook on Synchrotron Radiation", E.-E. Koch (ed.), North Holland, Amsterdam, 1983.
95. Special issue of J.Micr. 138, 229-331 (1985). Eleven papers on X-ray

microscopy.
96. J.C. Solem, Los Alamos National Laboratory report LA-9508-MS (1982). This paper contains definitions of "average" compositions of protein, DNA, lipid and carbohydrate that are convenient for calculations and are used where needed throughout the present work.
97. J.C. Solem, G.C. Baldwin, Science, 218, 229 (1982).
98. J.C. Solem, G.F. Chapline, Opt. Eng. 23, 193 (1984).
99. W.S. Haddad, D. Cullen, K. Boyer, C.K. Rhodes, J.C. Solem, R.S. Weinstein in "X-ray Microscopy II", op.cit., ref 6.
100. J.E. Trebes, S.B. Brown, E.M. Campbell, D.C. Matthews, D.G. Nilson, G.F. Stone, D.A. Whelan, Science, 238, 517 (1987).
101. R.A. London, J.E. Trebes, M.D. Rosen, op.cit., ref. 77.

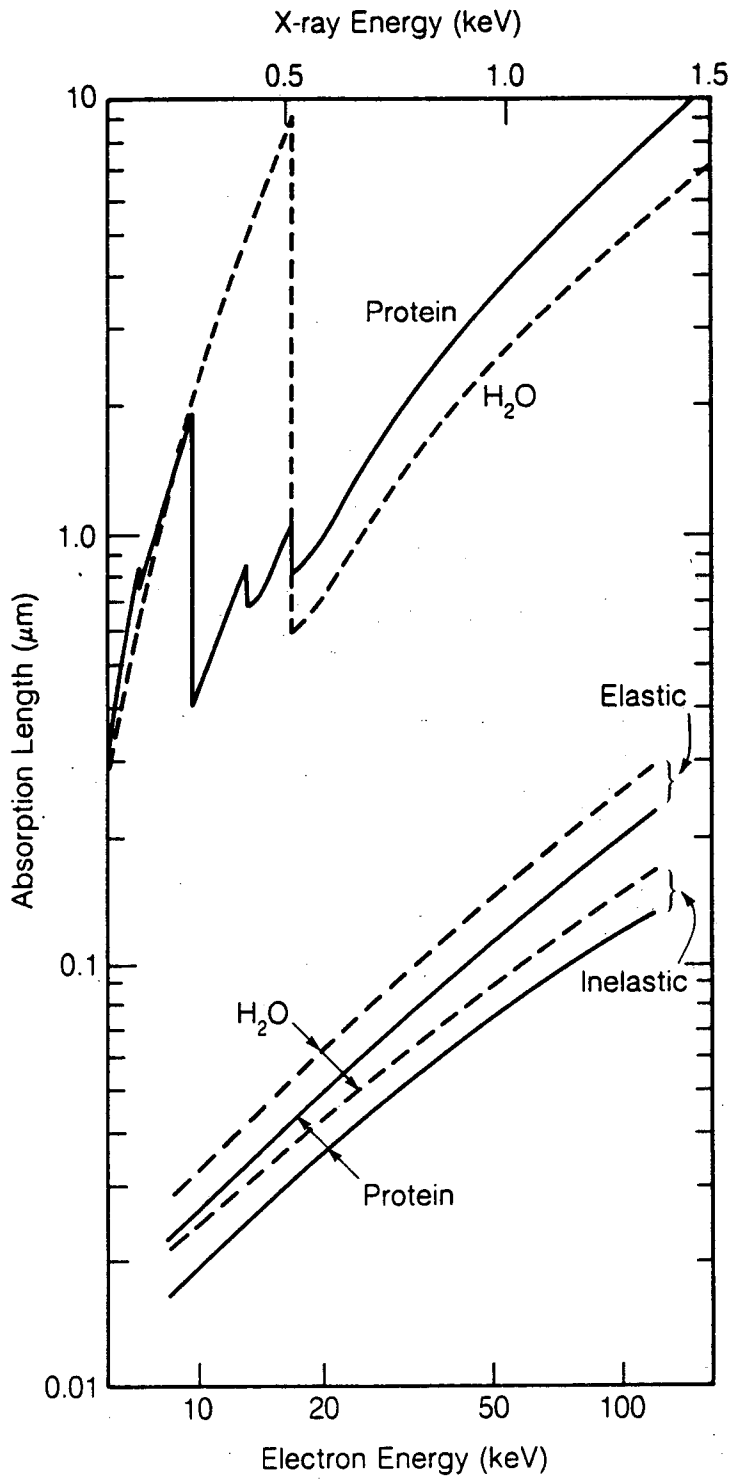

XBL 8411-5961

Fig. 1

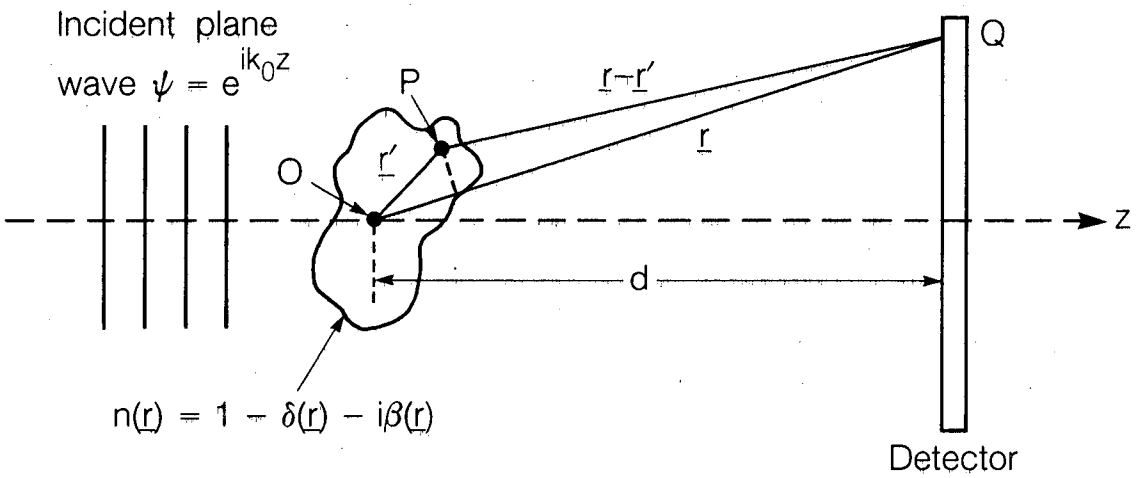

XBL 8411-5959A

Fig. 2

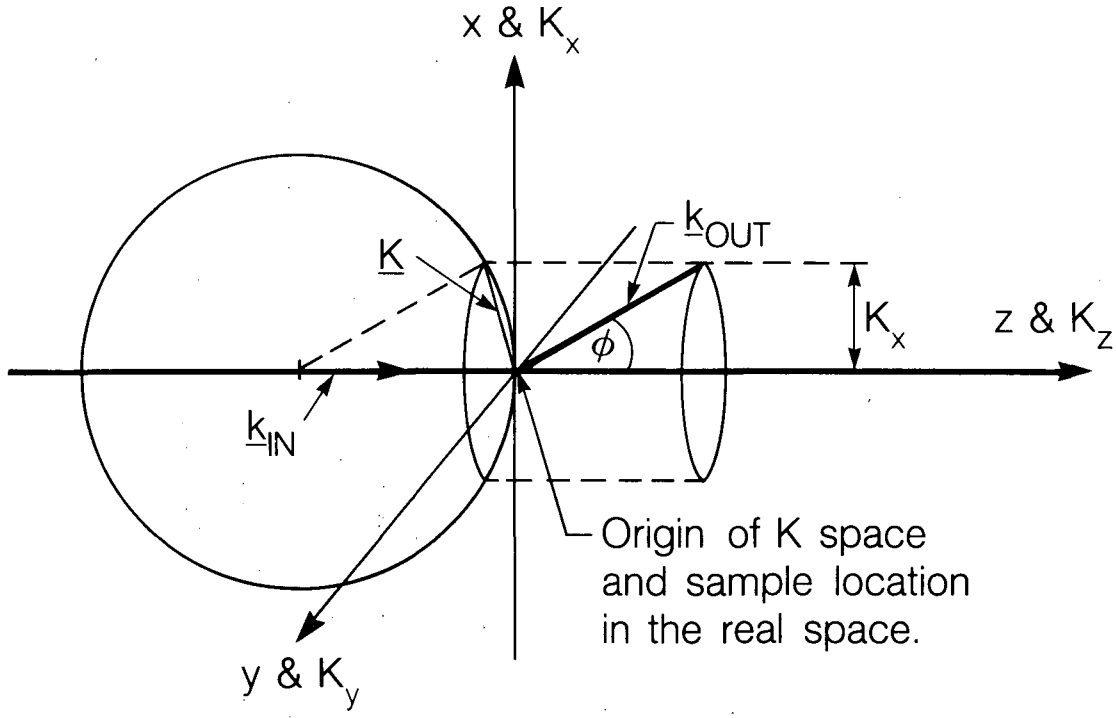

XBL 863-9788

Fig. 3

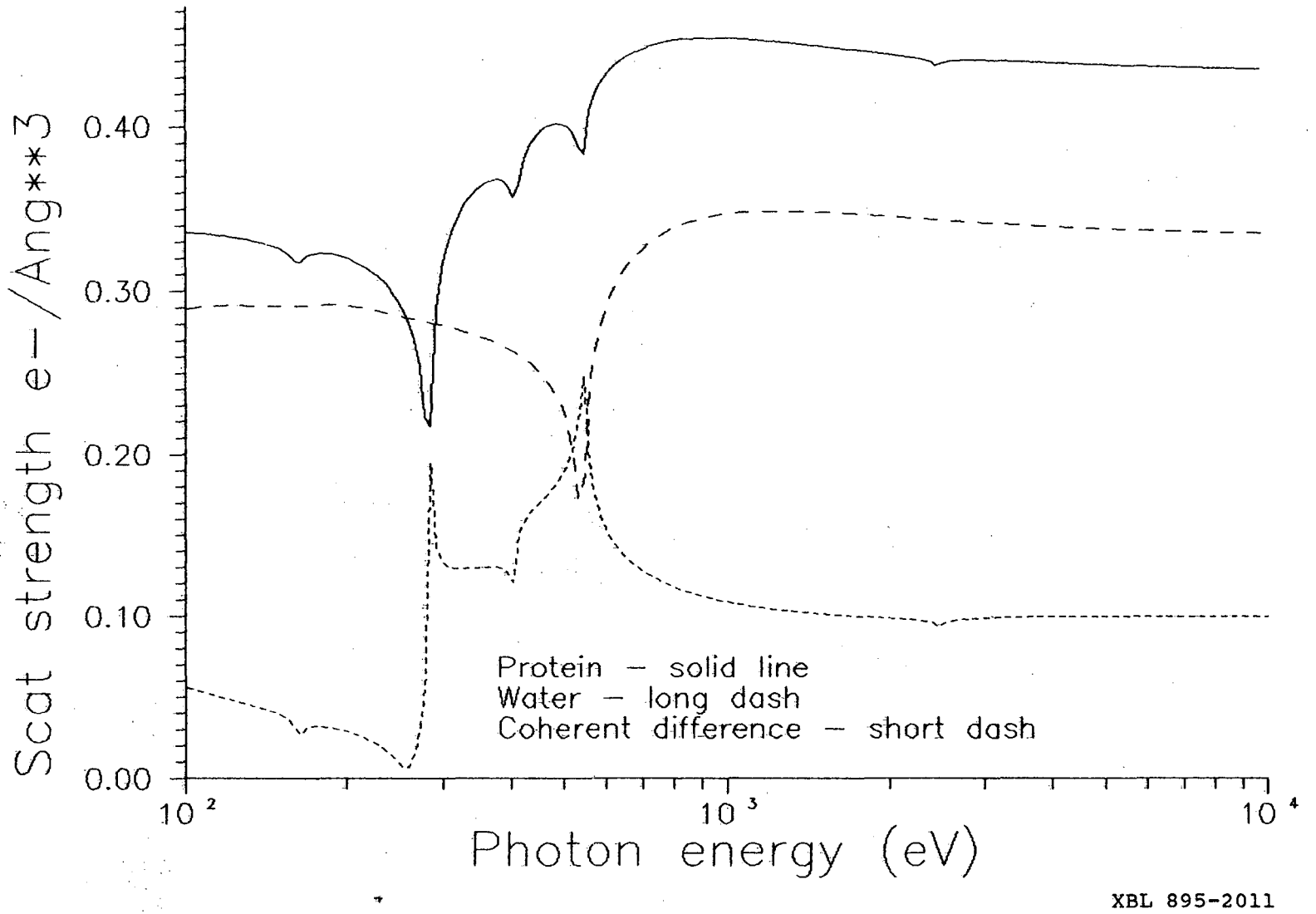
Scat strength e−/Ang**3
0.40
0.30
0.20
0.10
0.00
10 2
10 3
10 4
Photon energy (eV)
Protein − solid line
Water − long dash
Coherent difference − short dash
XBL 895-2011

Fig. 4

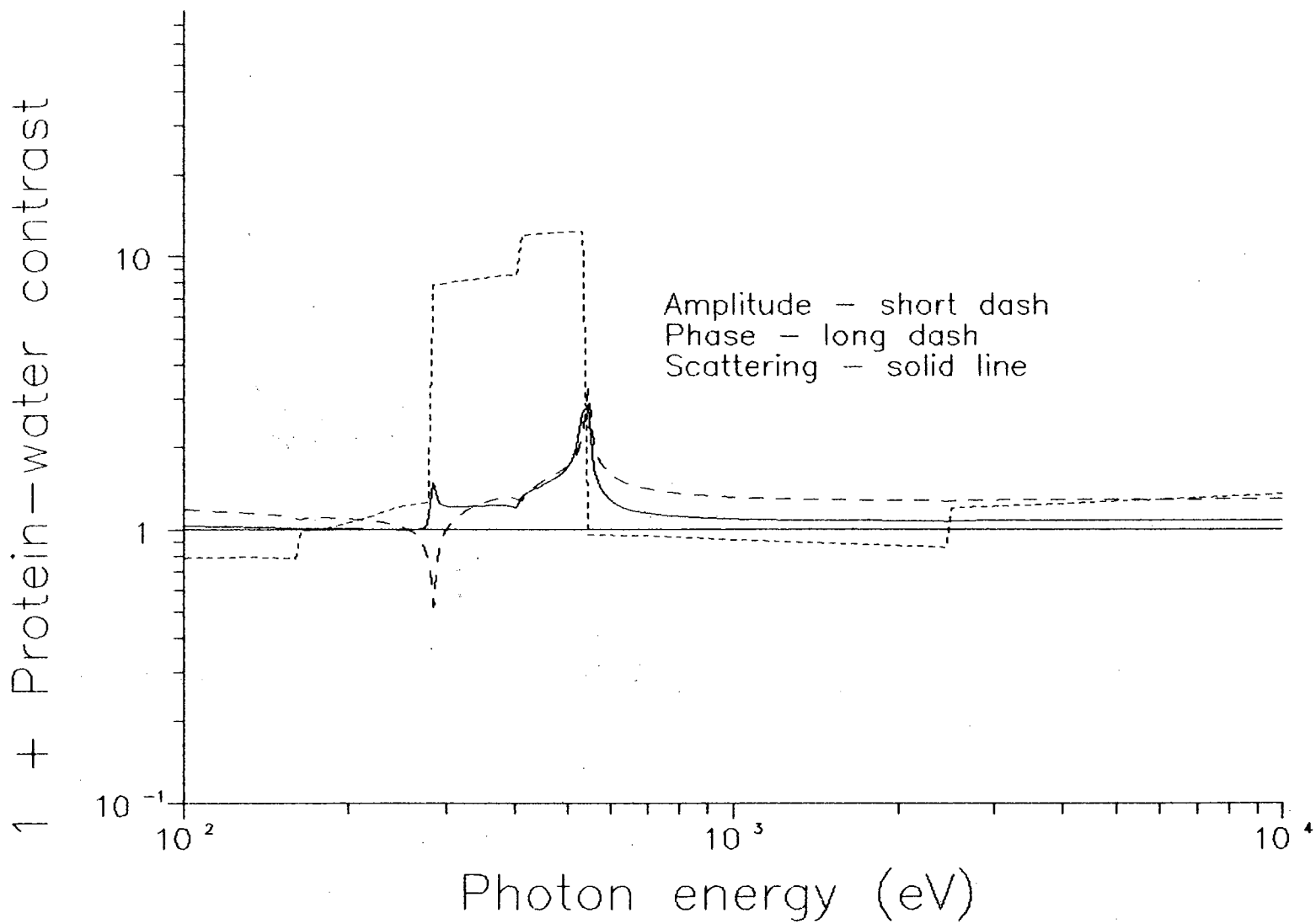

XBL 895-2009

Fig. 5

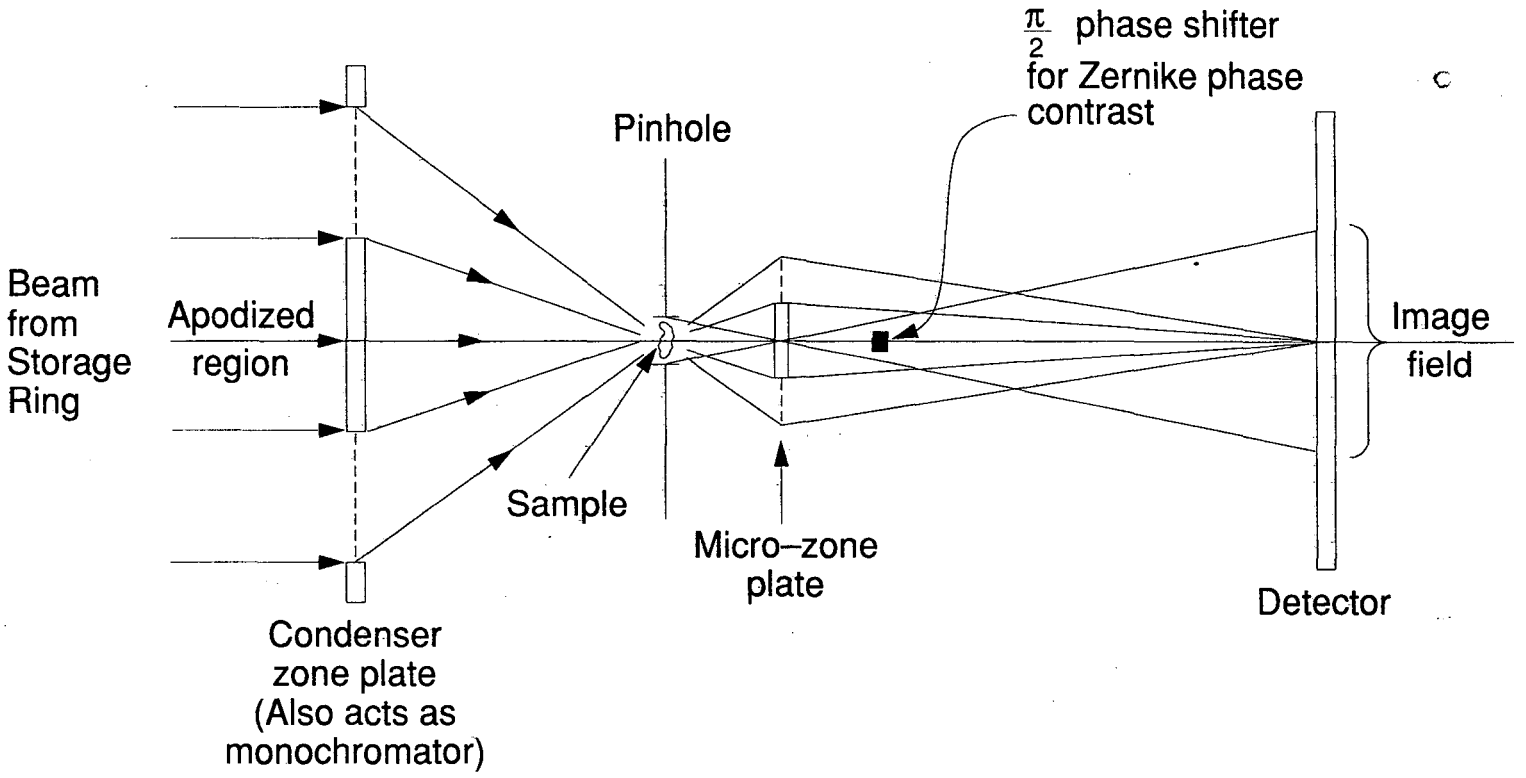

XBL 895–6020

Fig. 6

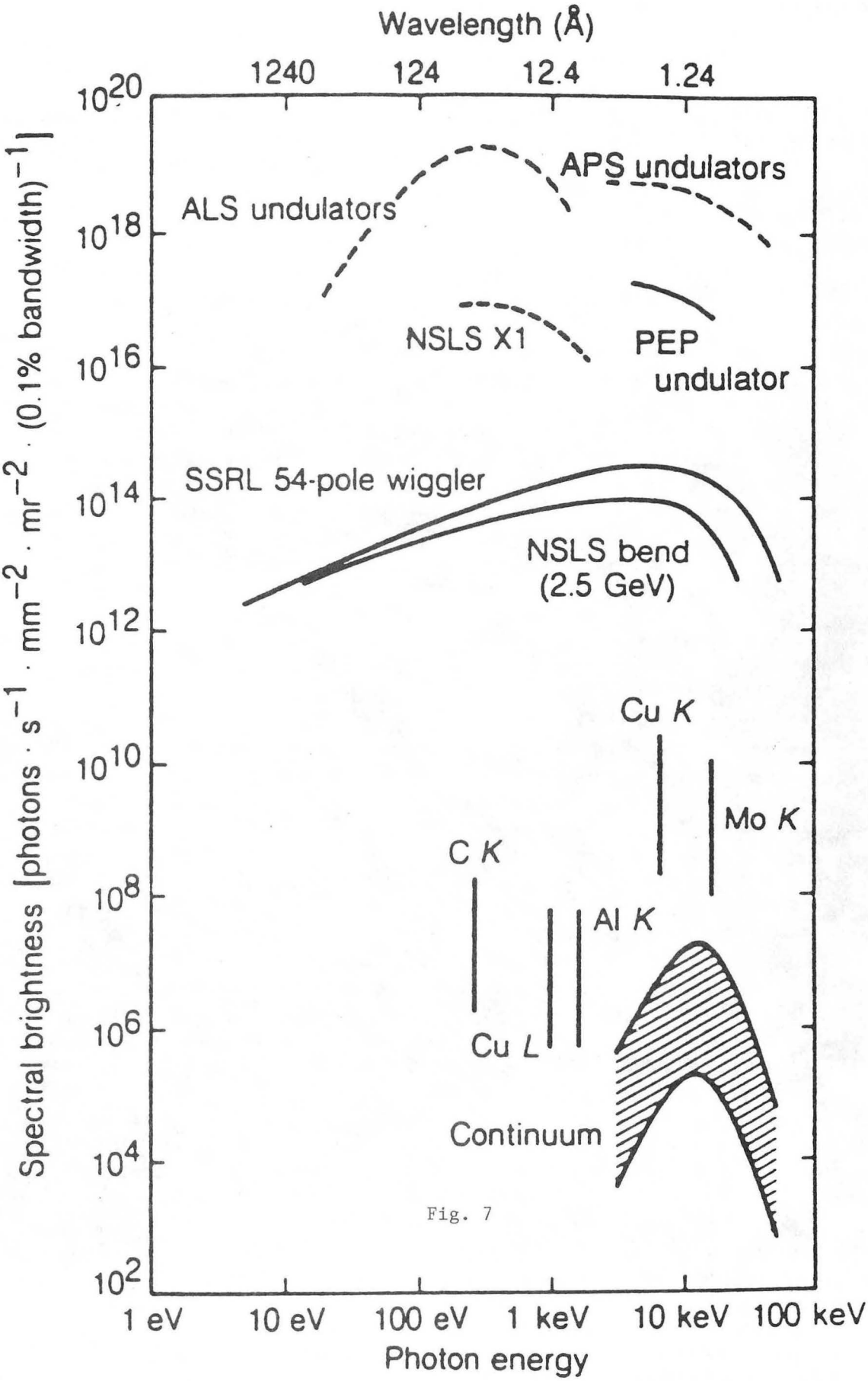
Wavelength (Å)
1240
124
12.4
1.24
10^{20}
10^{18}
10^{16}
10^{14}
10^{12}
10^{10}
10^{8}
10^{6}
10^{4}
10^{2}
Spectral brightness [photons · s^{-1} · mm^{-2} · mr^{-2} · (0.1% bandwidth)$^{-1}$]
ALS undulators
APS undulators
NSLS X1
PEP
undulator
SSRL 54-pole wiggler
NSLS bend
(2.5 GeV)
Cu K
Mo K
C K
Al K
Cu L
Continuum
1 eV
10 eV
100 eV
1 keV
10 keV
100 keV
Photon energy

Fig. 7

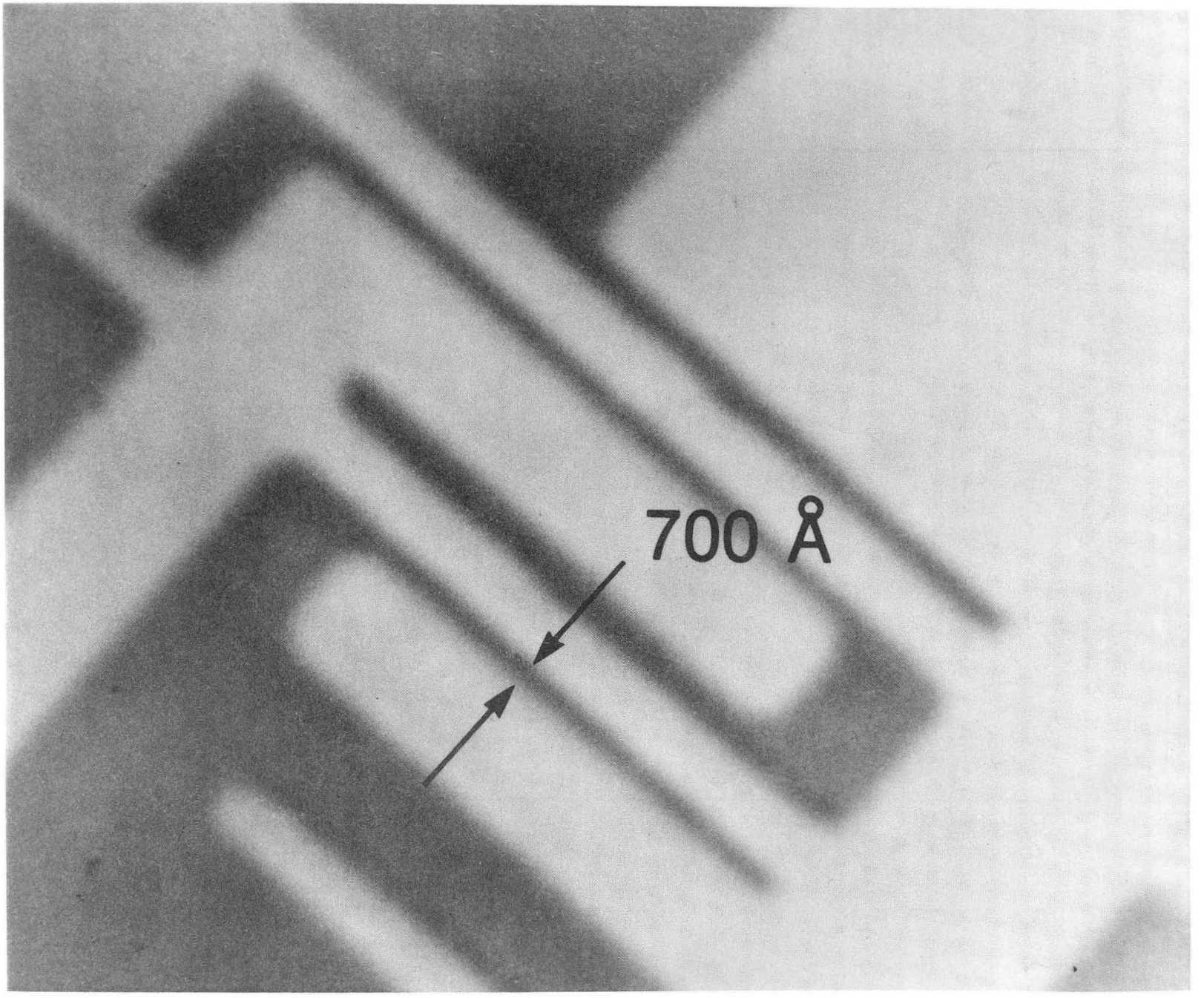

XBB 884-2781A

Fig. 8

Principle of The Scanning X–Ray Microscope

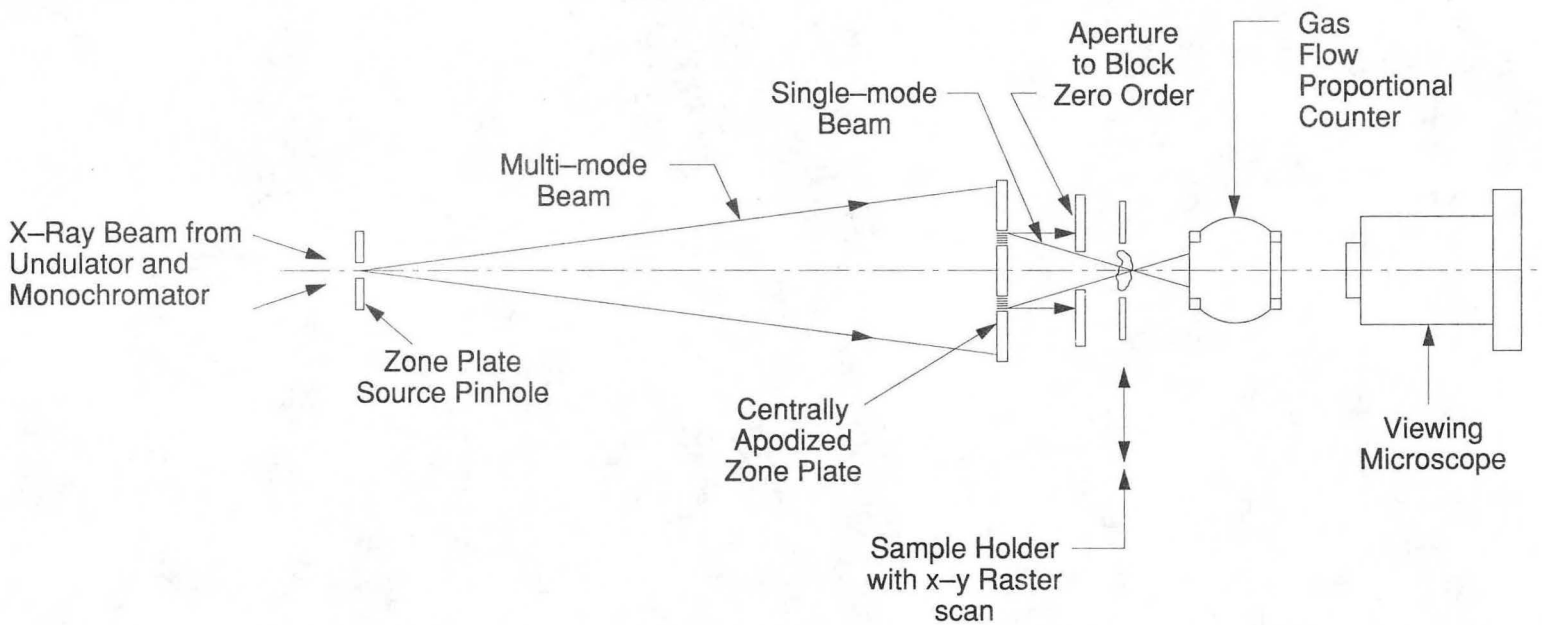

XBL 895–6019

Fig. 9

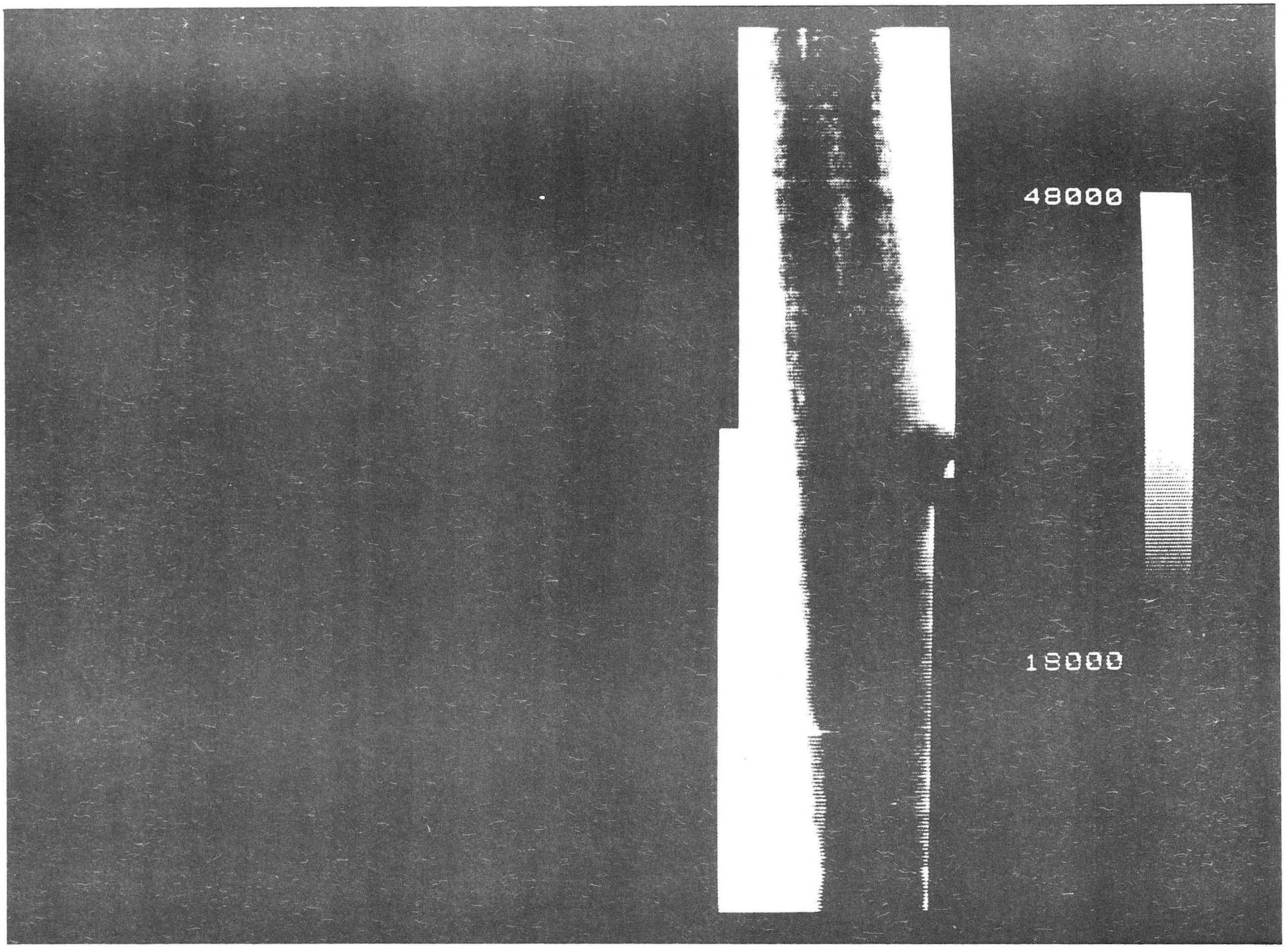

Fig. 10

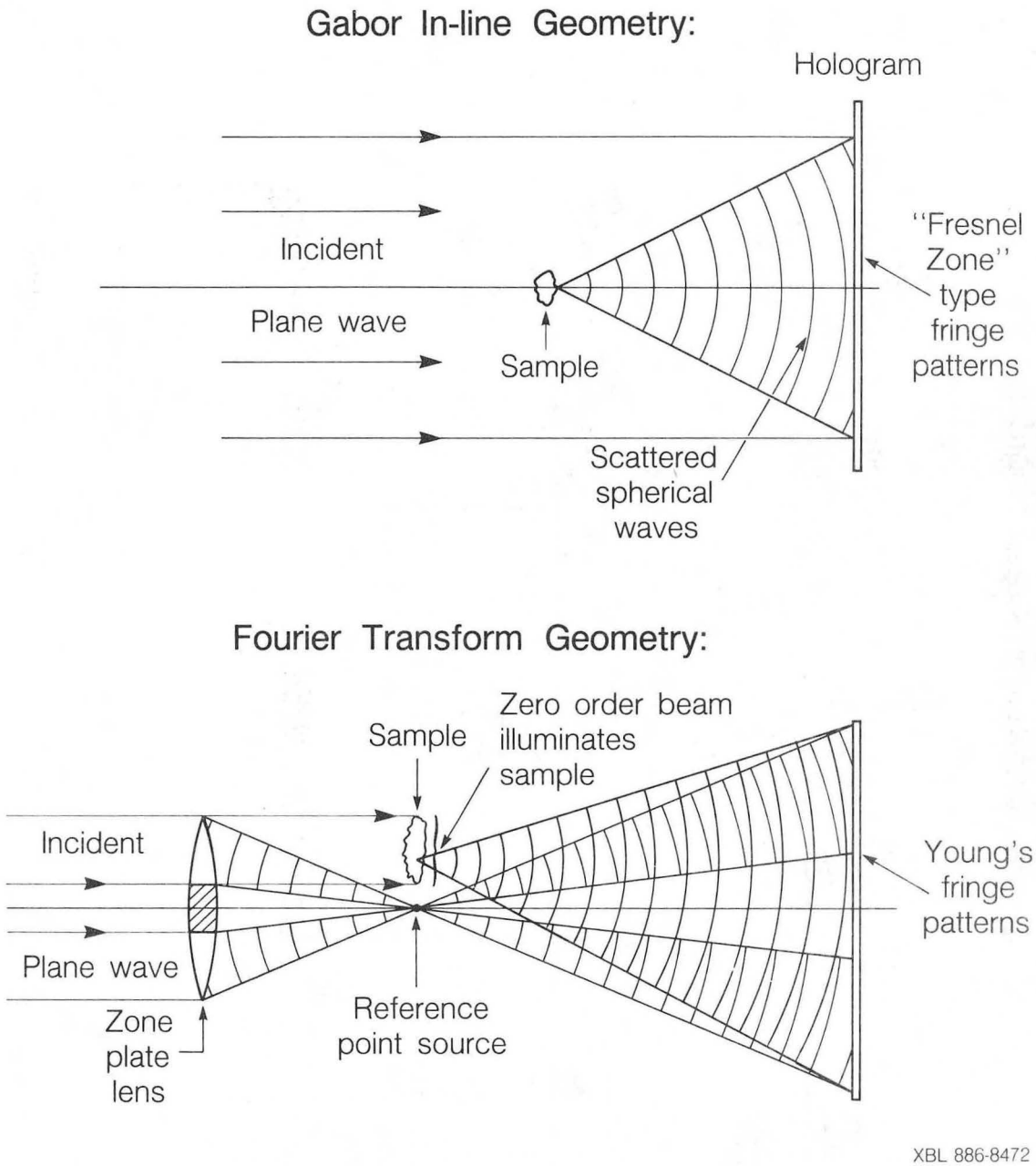
Gabor In-line Geometry:
Hologram
Incident
Plane wave
Sample
"Fresnel Zone" type fringe patterns
Scattered spherical waves
Fourier Transform Geometry:
Sample
Zero order beam illuminates sample
Incident
Plane wave
Young's fringe patterns
Zone plate lens
Reference point source
XBL 886-8472

Fig. 11

Optical System for X-ray holography

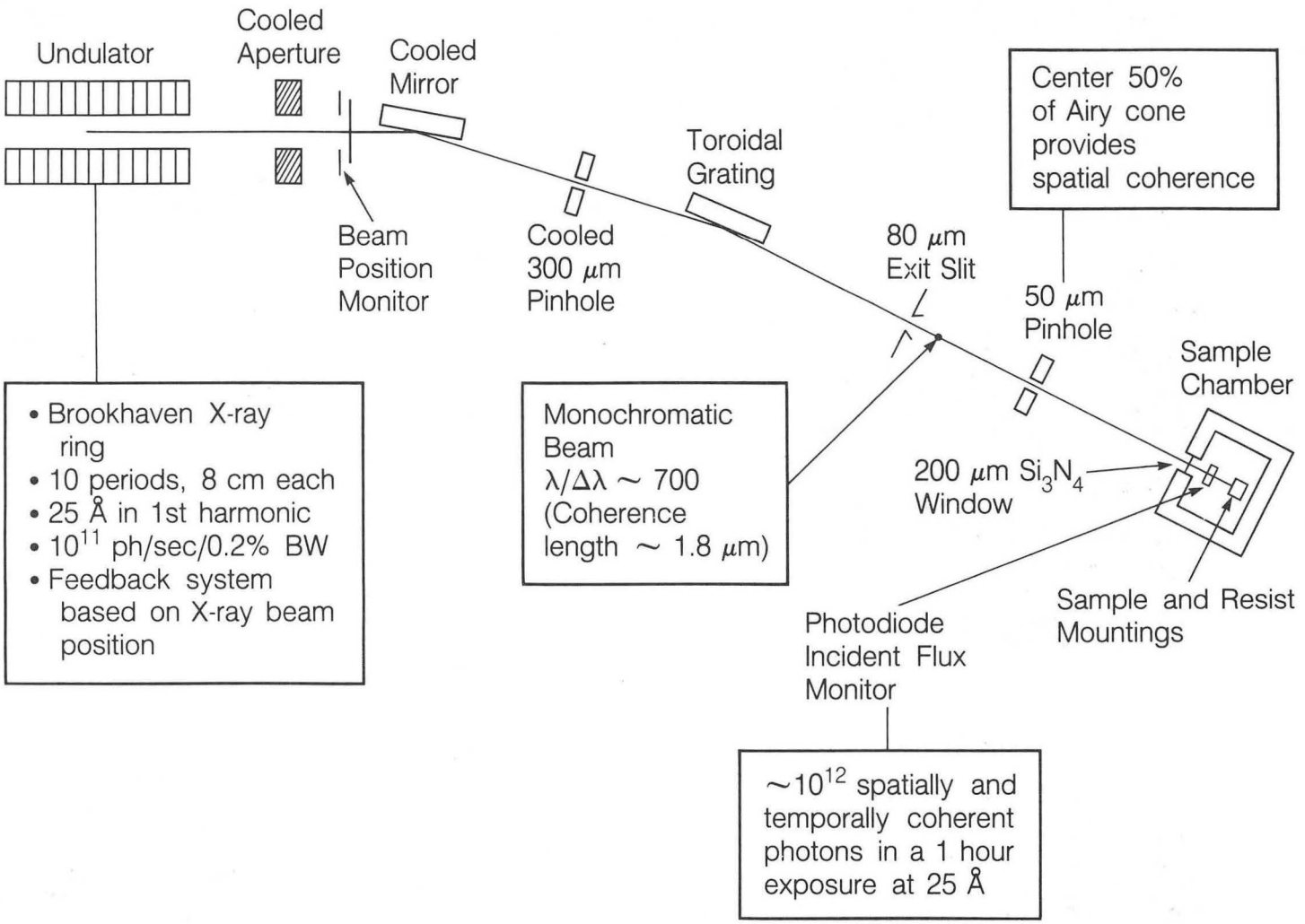

XBL 872-8109

Fig. 12

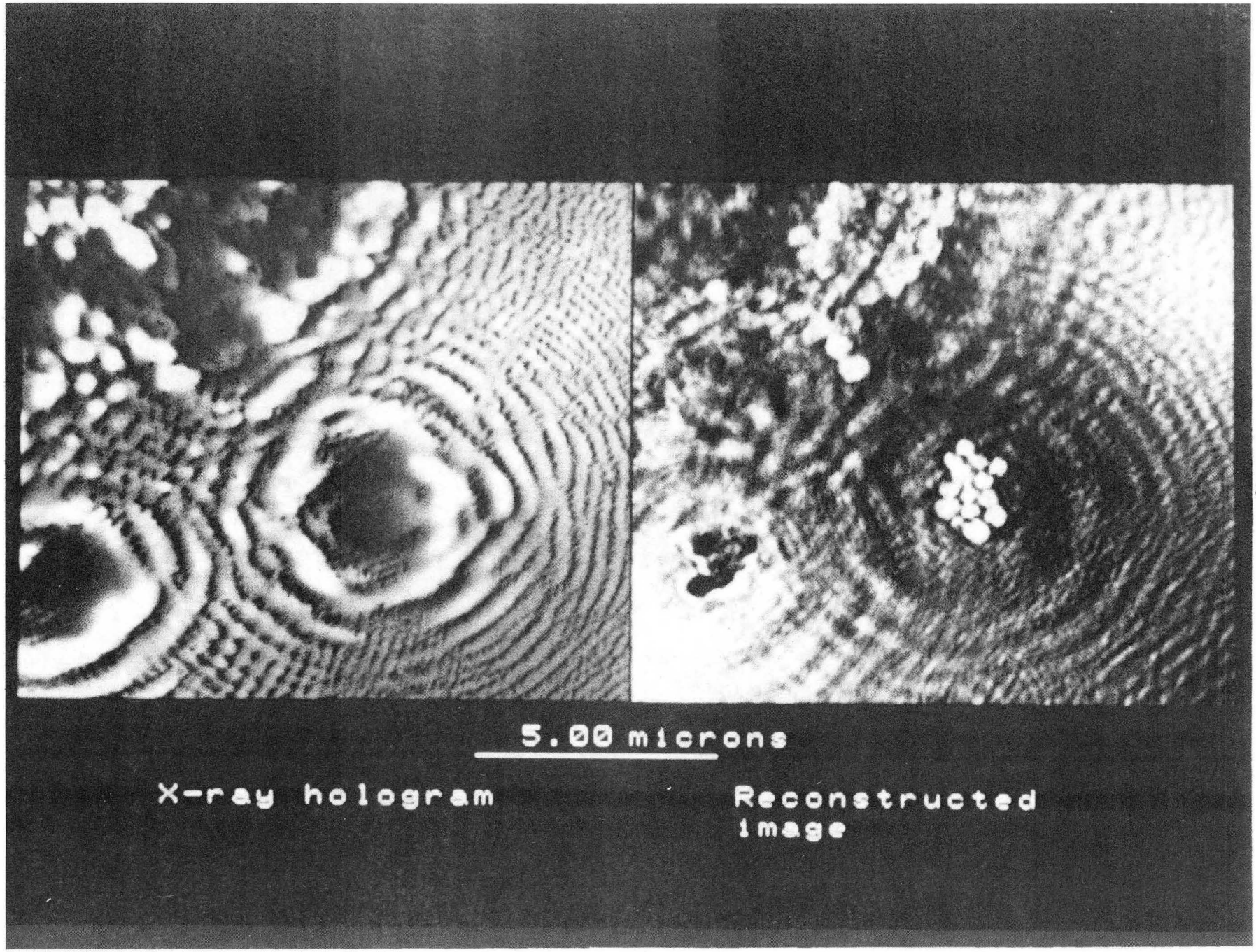

Fig. 13

XBB 884-3072

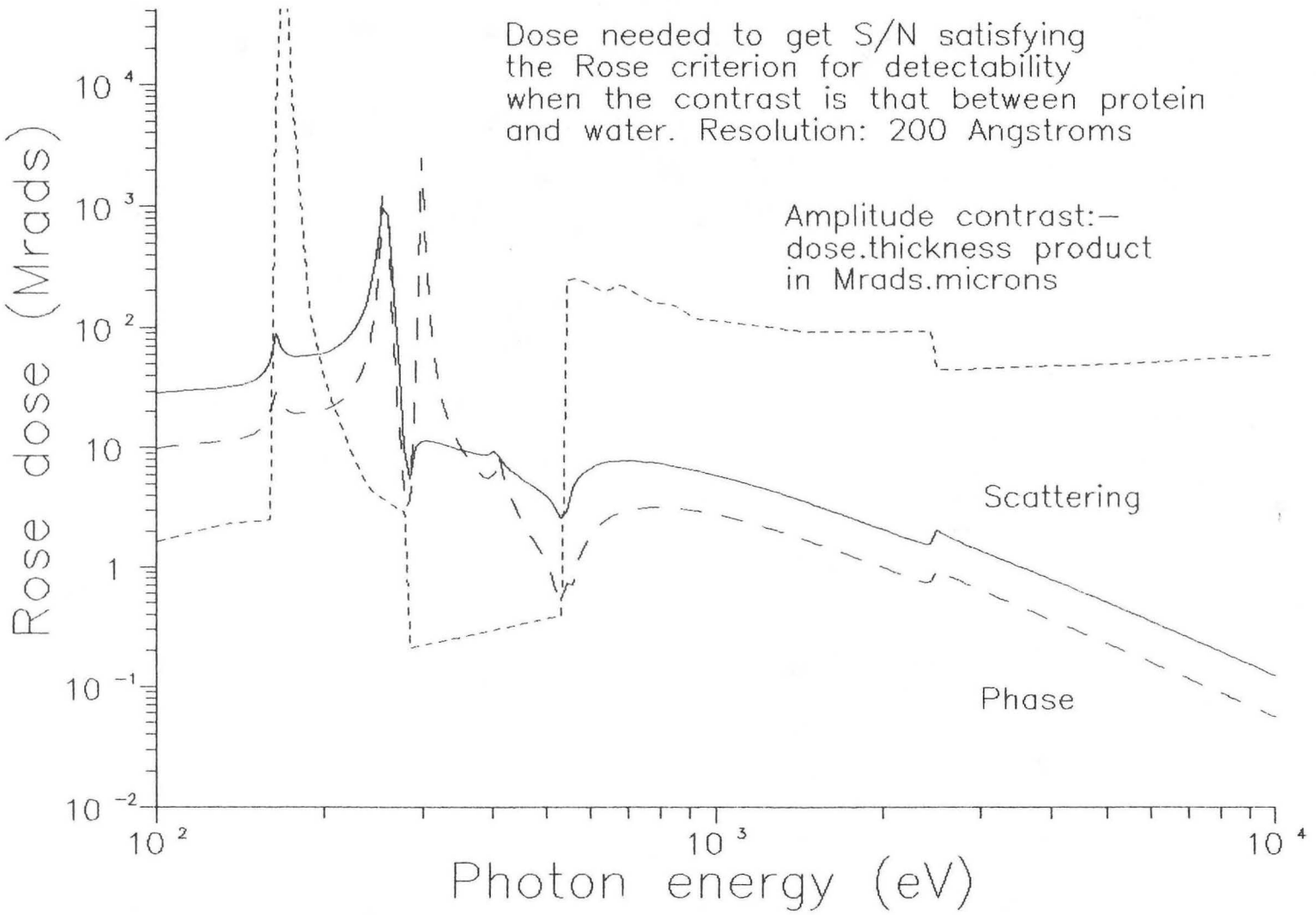

XBL 895-2010

Fig. 14